



HAL
open science

Vancomycin-decorated microbubbles as a theranostic agent for *Staphylococcus aureus* biofilms

Joop J.P. Kouijzer, Kirby Lattwein, Inés Beekers, Simone A.G. Langeveld, Mariël Leon-Grooters, Jean-Marc Strub, Estefania Oliva, Gaëtan L.A. Mislin, Nico de Jong, Antonius F.W. van Der Steen, et al.

► To cite this version:

Joop J.P. Kouijzer, Kirby Lattwein, Inés Beekers, Simone A.G. Langeveld, Mariël Leon-Grooters, et al.. Vancomycin-decorated microbubbles as a theranostic agent for *Staphylococcus aureus* biofilms. *International Journal of Pharmaceutics*, 2021, pp.121154. 10.1016/j.ijpharm.2021.121154. hal-03374256

HAL Id: hal-03374256

<https://hal.science/hal-03374256v1>

Submitted on 12 Oct 2021

HAL is a multi-disciplinary open access archive for the deposit and dissemination of scientific research documents, whether they are published or not. The documents may come from teaching and research institutions in France or abroad, or from public or private research centers.

L'archive ouverte pluridisciplinaire **HAL**, est destinée au dépôt et à la diffusion de documents scientifiques de niveau recherche, publiés ou non, émanant des établissements d'enseignement et de recherche français ou étrangers, des laboratoires publics ou privés.

Vancomycin-decorated microbubbles as a theranostic agent for *Staphylococcus aureus* biofilms

Joop J.P. Kouijzer^{1#}, Kirby R. Lattwein¹, Inés Beekers¹, Simone A.G. Langeveld¹, Mariël Leon-Grooters¹, Jean-Marc Strub², Estefania Oliva³, Gaëtan L.A. Mislin⁴, Nico de Jong^{1,5}, Antonius F.W. van der Steen^{1,5}, Alexander L. Klibanov⁶, Willem J.B. van Wamel⁷, Klazina Kooiman¹

1 Department of Biomedical Engineering, Thoraxcenter, Erasmus MC University Medical Center Rotterdam, Rotterdam, the Netherlands
Postal address: Office Ee2302, P.O. Box 2040, 3000 CA Rotterdam, the Netherlands

2 CNRS/University of Strasbourg UMR 7178, Institut Pluridisciplinaire Hubert Curien, Laboratoire de Spectrométrie de Masse Bio-Organique, Strasbourg-Cedex, France
Postal address: 25 rue Becquerel, F-67087 Strasbourg-Cedex 2, France

3 Faculté de Pharmacie de Strasbourg, Plateforme d'Analyse Chimique de Strasbourg-Illkirch (PACSI), Illkirch-Graffenstaden, France
Postal address: 74 route du Rhin, F-67400 Illkirch-Graffenstaden, France

4 CNRS/University of Strasbourg UMR7242, Illkirch-Graffenstaden, France
Postal address: 300 Boulevard Sébastien Brant, F-67400 Illkirch-Graffenstaden, France

5 Laboratory of Acoustical Wavefield Imaging, Faculty of Applied Sciences, Delft University of Technology, Delft, the Netherlands
Postal address: Building 22, Room D218, Lorentzweg 1, 2628 CJ Delft, the Netherlands

6 Cardiovascular Division, Department of Medicine, University of Virginia, Charlottesville, Virginia, United States of America
Postal address: UVA CVRC, PO Box 801394, Charlottesville, Virginia 22908, USA

7 Department of Medical Microbiology and Infectious Diseases, Erasmus MC, Rotterdam, the Netherlands
Postal address: Office Na9182, P.O. Box 2040, 3000 CA Rotterdam, the Netherlands

#Corresponding author: Joop J.P. Kouijzer, email: j.kouijzer@erasmusmc.nl, phone: +31 10 704 4633

Abbreviations

cMB: control microbubble; DiD: 1,1'-dioctadecyl-3,3',3'-tetramethylindodicarbocyanine perchlorate; DiI: 1,1'-Dioctadecyl-3,3',3'-Tetramethylindodicarbocyanine Perchlorate; DSPC: 1,2-distearoyl-*sn*-glycero-3-phosphocholine; fps: frames per second; IMDM: Iscove's Modified Dulbecco's Media; MALDI-TOF MS: matrix-assisted laser desorption/ionization - time-of-flight mass spectrometry; MW: molecular weight; NHS: *N*-hydroxysuccinimide; PBS: phosphate buffered saline; PEG: polyethylene-glycol; PI: propidium iodide; TLC: thin-layer chromatography; vMB: vancomycin-decorated microbubble.

1 **Abstract**

2 Bacterial biofilms are a huge burden on our healthcare systems worldwide. The lack of specificity in
3 diagnostic and treatment possibilities result in difficult-to-treat and persistent infections. The aim of this
4 *in vitro* study was to investigate if microbubbles targeted specifically to bacteria in biofilms could be used
5 both for diagnosis as well for sonobactericide treatment and demonstrate their theranostic potential for
6 biofilm infection management. The antibiotic vancomycin was chemically coupled to the lipid shell of
7 microbubbles and validated using mass spectrometry and high-axial resolution 4Pi confocal microscopy.
8 Theranostic proof-of-principle was investigated by demonstrating the specific binding of vancomycin-
9 decorated microbubbles (vMB) to statically and flow grown *Staphylococcus aureus* (*S. aureus*) biofilms
10 under increasing shear stress flow conditions (0-12 dyn/cm²), as well as confirmation of microbubble
11 oscillation and biofilm disruption upon ultrasound exposure (2 MHz, 250 kPa, and 5,000 or 10,000
12 cycles) during flow shear stress of 5 dyn/cm² using time-lapse confocal microscopy combined with the
13 Brandaris 128 ultra-high-speed camera. Vancomycin was successfully incorporated into the microbubble
14 lipid shell. vMB bound significantly more often than control microbubbles to biofilms, also in the
15 presence of free vancomycin (up to 1,000 µg/mL) and remained bound under increasing shear stress flow
16 conditions (up to 12 dyn/cm²). Upon ultrasound insonification biofilm area was reduced of up to 28%, as
17 confirmed by confocal microscopy. Our results confirm the successful production of vMB and support
18 their potential as a new theranostic tool for *S. aureus* biofilm infections by allowing for specific bacterial
19 detection and biofilm disruption.

20
21 **Keywords:** Biofilm, sonobactericide, targeted microbubble, theranostic, ultrasound, vancomycin

22 **1. Introduction**

23 Approximately 80% of all bacterial infections are associated with biofilms [1], where bacteria encase
24 themselves in a protective matrix hindering antibiotic effectiveness up to 1,000-fold compared to free-
25 floating (i.e., planktonic) bacteria and facilitating development of antibiotic resistance [2, 3]. This
26 increased resistance is largely due to the reduced metabolic activity of biofilm-embedded bacteria and the
27 limited penetration of antibiotics throughout the biofilm [4-6]. These life-threatening infections are
28 challenging to diagnose and treat, and are increasing in prevalence alongside the vulnerable aging
29 population and surging use of implantable life-saving/enhancing technologies that create niches primed
30 for colonization [7, 8]. Furthermore, biofilm infections are difficult to cure, often requiring high-risk,
31 costly, invasive procedures and can still become persistent, necessitating lifelong antibiotic use and/or
32 repeated medical interventions. Biofilm infections can occur anywhere in all organ systems and can carry
33 a high mortality rate depending on the location and infecting microbe. For example, infective endocarditis
34 is an infection of the heart valves and/or endocardial surface with an in-hospital mortality of 18-47.5% [9,
35 10] and a 5-year mortality of 40-69% [11-14]. Delayed diagnosis of infective endocarditis is associated
36 with increased mortality and early diagnosis of biofilm infection is therefore critical [11, 15, 16].
37 Currently there is no theranostic tool available in the clinic which combines the detection of biofilms with
38 treatment possibilities. A novel theranostic agent to detect early biofilm formation with subsequent
39 treatment possibilities would be a major breakthrough.

40 Microbubbles (1 – 10 μm in diameter) are ultrasound contrast agents that consist of an inert-gas core
41 encapsulated by a protein, phospholipid, or biocompatible polymer shell [17, 18] and used in daily
42 clinical practice for several decades to aid in the ultrasound diagnosis of cardiovascular diseases and
43 cancer [17, 19-21]. Their therapeutic potential, however, has only begun being substantiated with clinical
44 trials over the past years [22-25]. Microbubbles respond volumetrically, i.e., oscillate, to the increase and
45 decrease of pressure from ultrasonic waves [17, 18], and it is these ultrasound-activated responses that
46 enable them to be detected as well as induce various bioeffects for potential therapeutic applications.

47 Promising pre-clinical investigations have only recently begun to determine if microbubble-mediated
48 effects can be used to treat bacterial infections, which is referred to as sonobactericide [26]. Until now,
49 biofilms both grown and then treated under flow with sonobactericide have yet to be investigated, which
50 would be physiologically relevant for infections situated in flow environments.

51 Targeted microbubbles are microbubbles that have a ligand incorporated into their coating so they can
52 specifically bind to biomarkers, and have been extensively studied for their theranostic potential in
53 regards to mammalian cells [27]. Preclinically, targeted microbubble binding under flow conditions has
54 been used for the diagnosis of atherosclerosis [28], while clinical studies have shown the potential of
55 ultrasound molecular imaging of cancer [29, 30]. Treatment of different diseases was more effective with
56 targeted than with non-targeted microbubbles in *in vitro* and *in vivo* studies [19, 31]. To the best of our
57 knowledge, targeted microbubbles for biofilms have been investigated only once before, which was for
58 the detection of *Staphylococcus aureus* (*S. aureus*) biofilms using a monoclonal immunoglobulin
59 antibody to protein A (*S. aureus* bacterial cell wall surface protein) or a *Pseudomonas aeruginosa* lectin
60 [32]. Although these microbubbles successfully bound to the biofilms, the clinical translation is poor
61 because the antibody to protein A must compete with host antibodies that already bind to protein A for
62 immune surveillance/clearance and the *P. aeruginosa* lectin causes red blood cell agglutination [33, 34].

63 The purpose of this proof-of-principle study was to develop a clinically translatable novel theranostic
64 agent using vancomycin-decorated microbubbles (vMB) for the detection and treatment of clinically
65 relevant bacteria-associated biofilms. The antibiotic vancomycin was chosen as the ligand for its 1) 1)
66 binding ability to the D-Ala-D-Ala moiety ($K_D \sim 1 - 4 \mu\text{M}$) present in most gram-positive bacterial cell
67 walls [35], 2) potential for clinical application, and 3) possibility to covalently couple this compound
68 without losing its functionality (Fig. 1) [36]. Vancomycin was chemically coupled to the microbubble
69 coating via the functionalized polyethylene-glycol (PEG) conjugated lipid (DSPE-PEG(3400)) and
70 confirmed with matrix-assisted laser desorption/ionization - time-of-flight mass spectrometry (MALDI-
71 TOF MS), thin-layer chromatography (TLC), and 4Pi microscopy imaging. To mimic physiological
72 conditions, a biofilm flow model was grown and treated under physiological shear stress conditions using

73 an Ibidi microchannel flow set-up. We investigated the capability of the vMB to remain bound to
74 bacterial biofilms under static and shear stress conditions and evaluated their theranostic potential using
75 confocal microscopy combined with ultra-high-speed imaging using the Brandaris 128.

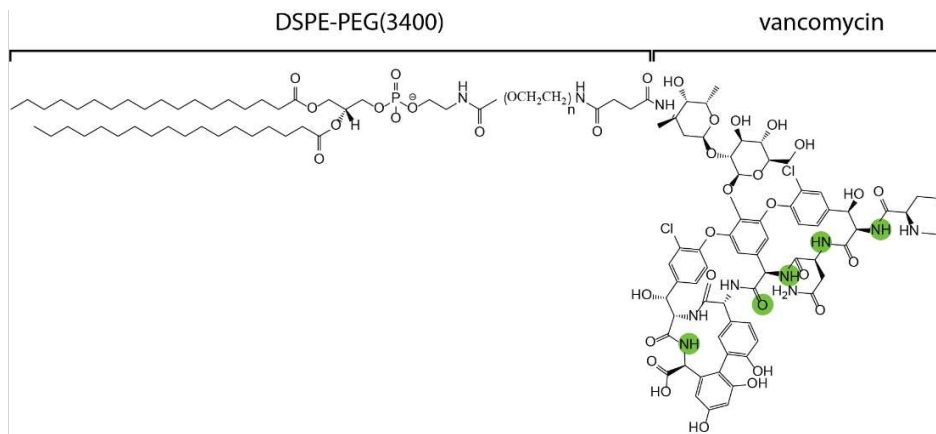
76 **2. Methods**

77 *2.1 Conjugation of vancomycin to phospholipid and incorporation in the microbubble shell*

78 *2.1.1 Vancomycin coupling to lipid DSPE-PEG(3400)-N-hydroxysuccinimide*

79 Thirty milligrams of DSPE-PEG(3400)-N-hydroxysuccinimide (DSPE-PEG(3400)-NHS; Sunbright
80 DSPE-034GS; NOF America Corporation, New York, USA or NOF Europe GmbH, Frankfurt am Main,
81 Germany) was dissolved in 1280 μ L dimethylsulfoxide (276855; Sigma-Aldrich, Saint. Louis, Missouri,
82 USA) for a final concentration of 23.4 mg/mL. The covalent coupling of vancomycin to DSPE-PEG-NHS
83 was performed as previously described for coupling of the cyclic RGD peptide [37], where the NHS ester
84 of DSPE-PEG reacts with the primary amino group of the peptide. The reaction mixture was made by
85 adding the DSPE-PEG(3400)-NHS solution to a 20% molar excess of vancomycin hydrochloride hydrate
86 (V0045000, Sigma-Aldrich) in dimethylsulfoxide. A 2-fold molar excess of *N,N*-diisopropylethylamine
87 (496219, Sigma-Aldrich) relative to the vancomycin hydrochloride hydrate was also added. The reaction
88 mixture was incubated on a rocker (15 rpm, PTR-35, Grant Instruments Ltd, Shepreth, United Kingdom)
89 overnight at room temperature. N-hydroxy succinimide, unreacted vancomycin, and byproducts were
90 removed by dialysis (Spectra/Por 1 Dialysis Membrane 6-8 kD; Spectrum, New Jersey, USA) in 500 mL
91 0.9% saline solution (Baxter International Inc., Deerfield, Illinois, USA) at 4 °C for 24 h. Then the saline
92 solution was replaced with 4 °C demi water every 24 h for two days. On the fourth day of dialysis, the
93 demi water was replaced twice with 4 h in between to reach the microSiemens value (Greisinger GMH
94 3431, Regenstauf, Germany) of demi water, i.e. 1-3 μ S. The final product (Fig. 1) was then freeze-dried
95 (Alpha 1-2 LD plus; Martin Christ GmbH, Osterode am Harz, Germany) and stored at -20 °C. Depending
96 on the supplier of the DSPE-PEG(3400)-NHS, the produced DSPE-PEG(3400)-vancomycin conjugate is

107 referred to as 'lipid conjugate (batch USA)', i.e. made from the DSPE-PEG(3400)-NHS obtained from
108 NOF America Corporation or 'lipid conjugate (batch EU)', i.e. made from DSPE-PEG(3400)-NHS
109 obtained from NOF Europe.



100

101 **Fig. 1.** Molecular structure of the functionalized polyethylene-glycol (PEG) conjugated lipid (DSPE-
102 PEG(3400)) coupled to the antibiotic molecule vancomycin. Green circles indicate where the vancomycin
103 interacts with the D-Ala-D-Ala moiety present in gram-positive bacterial cell walls [38].

104 2.1.2 Mass spectrometry

105 Electro spray ionization mass spectrometry experiments were performed on an Agilent Accurate Mass
106 QToF 6520 quadrupole time-of-flight instrument (Agilent Technologies, Santa Clara, CA, USA) based on
107 mass spectrometry analysis reported for similar compounds [39]. The electro spray ionization source was
108 operated in the positive ionization mode using a capillary voltage of 4500 V and the following conditions:
109 nebulizer nitrogen gas pressure, 10 psig; drying gas flow rate, 5 L/min; and drying temperature, 340 °C.
110 The scan range was m/z 50–3200 at 1 s/scan. Data acquisition was performed using MassHunter
111 Qualitative Analysis software (B.07.00, Agilent). Direct introduction conditions: samples were prepared
112 at a concentration of 1 mg/mL (in chloroform for the DSPE-PEG(3400)-NHS, lipid conjugate (batch
113 USA), and lipid conjugate (batch EU) and in water for vancomycin) and 1 μ L was injected. Injections

114 were done using acetonitrile as the mobile phase with a flow rate of 0.1 mL/min. MALDI-TOF Mass
115 measurements were carried out on an AutoflexTM MALDI-TOF mass spectrometer (Bruker Daltonics
116 GmbH, Bremen, Germany). This instrument was used at a maximum accelerating potential of 20 kV in
117 positive mode and was operated in linear mode. The delay extraction was fixed at 560 ns and the
118 frequency of the laser (nitrogen 337 nm) was set at 5 Hz. The acquisition mass range was set to 2,000-
119 8,000 m/z with a matrix suppression deflection (cut off) set to 1,500 m/z. The equipment was externally
120 calibrated with the single charge and double ion of insulin. Each raw spectrum was opened with
121 flexAnalysis 2.4 build 11 (Bruker Daltonics GmbH, Bremen, Germany) software and processed using the
122 following parameters: Savitzky-Golay algorithm for smoothing (width 5 and cycles 2), and sum algorithm
123 for peak detection and labelling. The matrix solution was prepared from a saturated solution of α -cyano-
124 4-hydroxycinnamic acid in water/acetonitrile 50/50. The sample (less than 0.1 mg) was suspended in 1
125 mL of chloroform, and then 1 μ L of the sample was added to 10 μ L of saturated matrix solution. The
126 mixture (1 μ L) was loaded on the target and dried at room temperature.

127 *2.1.3 Thin-layer chromatography*

128 TLC sheets (TLC Silica gel 60 F₂₅₄ Aluminum sheets; EMD Millipore Corporation, Burlington,
129 Massachusetts, USA) were used as a stationary phase. A mixture of chloroform and methanol in a 9:1 v/v
130 ratio was used as the mobile phase. DSPE-PEG(3400)-NHS and the lipid conjugate (batch USA and EU),
131 were dissolved in chloroform to a concentration of 25 mg/mL and vancomycin was dissolved in methanol
132 to a concentration of 25 mg/mL. Dissolved compounds were then spotted onto the TLC sheet using glass
133 capillaries. Sheets were inspected for compounds under UV light (VL-6M, Vilber Lourmat, Collégien,
134 France) after exposure to iodine vapors (207772; Thermo Fisher Scientific, Waltham, Massachusetts,
135 USA).

136 *2.1.4 Microbubble production*

137 To produce vMB, 1,2-distearoyl-*sn*-glycero-3-phosphocholine (DSPC, 12.5 mg/mL, 86.4 mol%;
138 Sigma-Aldrich), custom-made lipid conjugate (batch USA or EU) (4.35 mg dissolved as 2.9 mg/mL, 5.3
139 mol%), and PEG-40 stearate (12.5 mg/mL, 8.3 mol%; Sigma-Aldrich) were first dissolved in phosphate
140 buffered saline (PBS; 14200083; Thermo Fisher Scientific) saturated with perfluorobutane (C₄F₁₀; 355-
141 25-9, F2 Chemicals Ltd, Preston, Lancashire, UK) using a sonicator bath for 10 min. To fluorescently
142 label the vMB coating, the lipid dye DiD (1,1'-dioctadecyl-3,3,3',3'-tetramethylindodicarbocyanine
143 perchlorate; D307; Thermo Fisher Scientific) was added and mixed by probe sonication (Sonicator
144 Ultrasonic Processor XL2020, Heat Systems, Farmingdale, New York, USA) at 20 kHz at power level 3
145 for 3 min. This was followed by probe sonication for 60 s at power level 8 under continuous C₄F₁₀ gas
146 flow [40]. vMB were produced without the addition of lipid dye for ultrasound molecular imaging
147 experiments and determining the vancomycin concentration on vMB. Microbubbles were stored in sealed
148 30 mL glass vials (DWK Life Sciences GmbH, Mainz, Germany) under C₄F₁₀ atmosphere at 4 °C and
149 used within three days. To produce non-targeted control microbubbles (cMB), the custom-made lipid
150 conjugate was substituted for DSPE-PEG(3400) (2142-3400; Nanosoft Polymers, New York, USA). To
151 fluorescently label the cMB coating, the lipid dye DiD or DiI (1,1'-Dioctadecyl-3,3,3',3'-
152 Tetramethylindodicarbocyanine Perchlorate; D282; Thermo Fisher Scientific) was added before probe
153 sonication. Before experiments, microbubbles were washed three times with C₄F₁₀-saturated PBS by
154 centrifugation at 400 *g* for 1 min (Heraeus Biofuge Primo, Waltham, Massachusetts, USA). The
155 microbubble size distributions and concentrations were measured using a Coulter Counter Multisizer 3
156 (Beckman Coulter, Brea, California, USA). Particles (1 - 30 μm) were quantified using a 50 μm aperture
157 tube. To determine the vancomycin loading efficiency of the vMB, 1970 μL out of a total of 3260 μL
158 washed vMB (batch EU), were sonicated in a water bath for 10 min to destroy the microbubbles. This was
159 followed by freeze-drying (Martin Christ GmbH) which yielded 23.24 mg of destroyed freeze-dried vMB.
160 The destroyed freeze-dried vMB (4.65 and 3.83 mg) and corresponding lipid conjugate (batch EU; 0.79
161 and 0.48 mg) were dissolved in 50 μL and 350 μL Multi-Assay Manual Diluent (7D82P; Abbott
162 Laboratories, Chicago, Illinois, USA), respectively. The obtained solutions were inserted in the Architect

163 c4000 clinical chemistry analyzer (Abbott Laboratories) in combination with the Multigent vancomycin
164 reagents kit (6E44-21; Abbott Laboratories) to obtain the vancomycin concentration. The vMB loading
165 efficiency was defined by the following formula:

166
$$\text{Loading efficiency} = \frac{\text{vancomycin in 1 washed vMB batch}}{\text{vancomycin in 4.35 mg lipid conjugate}} \times 100\%$$

167 The amount of vancomycin molecules per μm^2 of microbubble shell was calculated by dividing the
168 amount of vancomycin on the vMB by the surface of the vMB: $4\pi N \sum_{i=1}^k x_i r_i^2$, where x_i is the number
169 fraction, r_i the radius of that fraction, and k the number of bins (as determined with the Coulter Counter).

170

171 *2.1.5 4Pi microscopy imaging*

172 vMB (lipid conjugate batch EU) and DiI-containing cMB were incubated with anti-vancomycin IgG
173 rabbit antibody coupled to a FITC-molecule ($1 \mu\text{g}/1 \times 10^8$ MBs; LS-C540056; LifeSpan BioSciences,
174 Seattle, Washington, USA) on ice for 30 min. To remove excess antibody, microbubbles were washed
175 with C_4F_{10} -saturated PBS as described above. Microbubbles were then placed in 87% glycerol (v/v in
176 PBS) to reduce Brownian motion. Y-stacked xz-scans were acquired using a Leica TCS 4Pi confocal
177 laser-scanning microscope with two aligned opposing objectives for high axial resolution (90 nm step
178 size, 100 \times glycerol HCX PL APO objective lens, numerical aperture 1.35). The FITC antibody was
179 excited using a 488 nm laser and detected at 500-550 nm. For lipid shell visualization, DiI and DiD were
180 excited with a 561 nm laser and detected at 580-640 nm and 647-703 nm, respectively. The 'voltex'
181 function in AMIRA software (Version 2020.1, FEI, M \acute{e} rignac Cedex, France) was used for rendering
182 volume projections of the acquired y-stacked xz-scans.

183 *2.2 Biofilm formation*

184 *2.2.1 Static biofilm formation*

185 An infective endocarditis patient-derived *S. aureus* bacterial strain, associated with cardiovascular
186 infections (ST398), was used for this study. This strain was collected by the department of Medical
187 Microbiology and Infectious Diseases, Erasmus MC University Medical Center Rotterdam, the
188 Netherlands, and anonymized and de-identified according to institutional policy. Frozen stock samples
189 were streaked onto tryptic soy agar containing 5% sheep blood (BD, Trypticase™, Thermo Fisher
190 Scientific) and allowed to grow overnight at 37 °C. Bacterial colonies were suspended in Iscove's
191 Modified Dulbecco's Media (IMDM; Gibco, Thermo Fisher Scientific) until an optical density of 0.5 (\pm
192 0.05) was reached at 600 nm (Ultraspec 10, Amersham Biosciences, Little Chalfont, United Kingdom)
193 corresponding to 1×10^8 colony forming units per mL (CFU/mL). IbiTreat polymer μ -Slides (80196; 0.8
194 mm channel height; I Luer; Ibidi GmbH, Gräfelfing, Germany) were inoculated with 200 μ L of diluted
195 bacterial suspension consisting of 1×10^4 CFU/mL. The IbiTreat μ -Slide in- and outlet-reservoirs were
196 filled with 60 μ L of IMDM. Slides were then incubated at 37 °C for 24 h in a humidified incubator under
197 constant agitation (150 rpm; Rotamax 120, Heidolph Instruments, Schwabach, Germany).

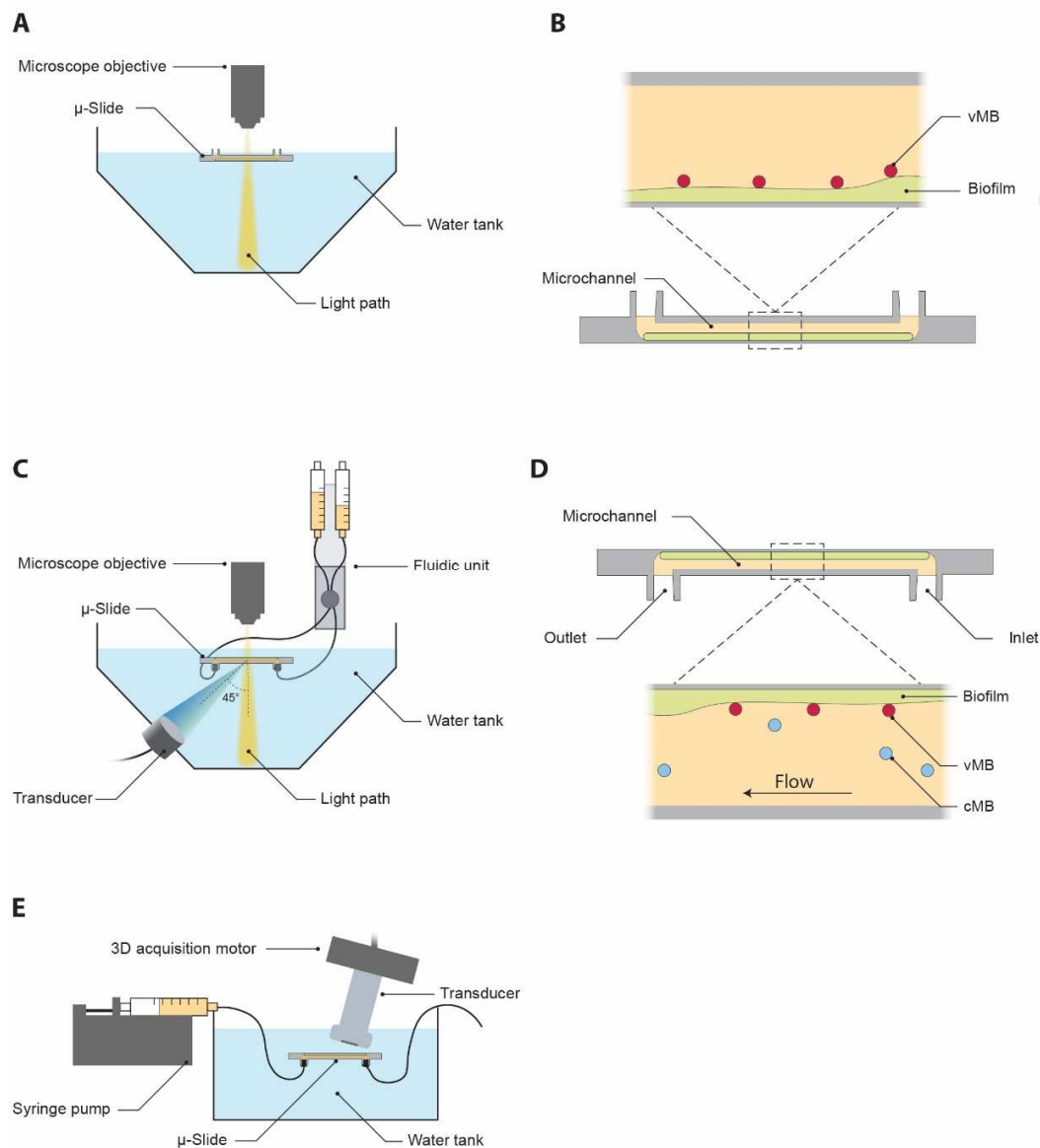
198 2.2.2 Biofilm formation under flow

199 IbiTreat μ -Slides were incubated with 320 μ L of type O human plasma (citrate phosphate double
200 dextrose as an anti-coagulant; pooled from five donors to minimize donor variability; Sanquin,
201 Rotterdam, the Netherlands) to aid bacterial attachment under flow. After incubation at 37 °C for 24 h in
202 a humidified incubator, plasma was removed and the slides were rinsed three times with 200 μ L 0.9%
203 saline solution (Baxter International). Then, an IMDM diluted *S. aureus* bacterial suspension of 200 μ L
204 containing 1×10^6 CFU/mL was pipetted into the slide. Bacteria were allowed to attach to the surface of
205 the μ -Slide for 3 h at 37 °C and then the μ -Slide was connected to an Ibidi fluidic unit using
206 corresponding perfusion sets (Perfusion set red, 10962; Ibidi) and a computer-controlled air pressure
207 pump (Ibidi pump system; Ibidi). In order to later on inject microbubbles and dyes, an in-line Luer
208 injection port (10820; Ibidi) was placed in the perfusion set 3.5 cm before the μ -Slide inlet. Biofilms were

209 grown under laminar flow at 5 dyn/cm^2 (14.4 mL/min, corresponding to a Reynolds number of 32) for 24
210 h at 37 °C.

211 *2.3 Experimental set-up*

212 The μ -Slides were inserted into a custom-built water tank, that was maintained at 37 °C and situated
213 underneath a custom-built Nikon A1R+ confocal microscope [41] (Nikon Instruments, Amsterdam, the
214 Netherlands) (Fig. 2A, C). The orientation of the μ -Slide was either upright (Fig. 2A-B) or flipped 180°
215 (Fig. 2C-D) depending on the experiment performed. The transducer (2.25 MHz center frequency used at
216 2 MHz; 76.2 mm focal length; -6 dB beam width of 3 mm at 2 MHz; V305; Panametrics-NDT, Olympus,
217 Waltham, MA, USA) was placed underneath the sample at a 45° angle to minimize ultrasound reflection
218 and standing wave formation. Both the optical and ultrasound foci were aligned using a pulse-echo
219 approach and a needle tip located at the optical focal plane [42], hereby the microbubbles and biofilm
220 could both be simultaneously imaged and insonified. An arbitrary waveform generator (33220A; Agilent),
221 in combination with a broadband amplifier (ENI A-500; Electronics & Innovation, Rochester, NY, USA),
222 was connected to the transducer. The transducer output was calibrated in a separate experiment using a
223 needle hydrophone (1 mm diameter; PA2293; Precision Acoustics, Dorchester, UK). As a live/dead
224 staining, SYTO 9 (S34854; Thermo Fisher Scientific) was excited at 488 nm and detected at 525/50 nm
225 (center wavelength/bandwidth) and propidium iodide (PI; P4864-10ML; Sigma-Aldrich) was excited at
226 561 nm and detected at 595/50 nm. For experiments with DiI incorporated into the cMB, the 561 nm laser
227 with the same detection was also used for optical imaging. A third channel was used for the visualization
228 of DiD incorporated into vMB or cMB with an excitation at 640 nm and fluorescence detected at 700/75
229 nm.



230 **Fig. 2.** Schematic representation (not drawn-to-scale) of the experimental set-ups for (A, B) the static
 231 experiments, (C, D) the flow experiments and (E) the ultrasound molecular imaging experiment. (B)
 232 Zoomed-in cross-section of the Ibidi μ -Slide in A and (D) zoomed-in cross-section of the μ -Slide in C,
 233 both indicating the placement of the biofilm within the microchannel containing vancomycin-decorated
 234 microbubbles (vMB, red) and control microbubbles (cMB, blue).

235 2.4 Binding of targeted microbubbles to bacteria in biofilms

236 2.4.1 Competitive microbubble binding assay

237 To study the competitive binding of vMB (lipid conjugate batch USA and EU), statically grown
 238 biofilms were pre-incubated at room temperature for 5 min with vancomycin concentrations of 0, 10, 20,

239 100 or 1,000 $\mu\text{g}/\text{mL}$ dissolved in IMDM. This includes the maximal recommended clinical blood level
240 concentration of vancomycin, i.e., 20 $\mu\text{g}/\text{mL}$ [43, 44]. A final vancomycin concentration of 0 or 1,000
241 $\mu\text{g}/\text{mL}$ was used in the μ -Slides for cMB. After this, the dyes (0.4 μL of 5 mM SYTO 9, 5 μL of 1.5 mM
242 PI) and fluorescent DiD microbubbles (7.0×10^5 vMB or cMB) were added to IMDM containing the same
243 pre-incubation vancomycin concentration to a total of 200 μL , which was then added to the μ -Slide
244 replacing the pre-incubation. Slides were flipped 180° for 5 min to allow the microbubbles to float up
245 towards the biofilm for binding at room temperature and then flipped back to their original position, such
246 that any unbound microbubbles would rise to the top of the channel (Fig. 2B). For each vancomycin
247 concentration, the binding assay was performed in at least three μ -slide. Slides were systematically
248 imaged with a $100\times$ water-dipping objective (CFI Plan 100XC W, Nikon Instruments) of which each
249 field-of-view consisted of 512×512 pixels ($128 \times 128 \mu\text{m}^2$). Locations within the slide were named 1 – 5
250 and were equally spaced apart, with 1 representing the field-of view nearest to the inlet and 5 nearest to
251 the outlet. The number of microbubbles attached to bacterial biofilms was manually determined using
252 Fiji software for 20 different fields-of-view (5 locations distributed over the length of the microchannel,
253 with 4 equally spaced fields-of-view per location) distributed over each μ -Slide.

254 2.4.2 Non-specific microbubble binding assay

255 For assessment of non-specific binding of microbubbles, μ -Slides with and without statically grown
256 biofilms were treated similarly. μ -Slides without biofilm were filled with 200 μL IMDM and in- and
257 outlet-reservoirs with 60 μL of IMDM. Slides were then incubated at 37°C for 24 h in a humidified
258 incubator under constant agitation (150 rpm). Before the binding assay, all μ -Slides were first rinsed by
259 adding 200 μL IMDM to the inlet and removing 200 μL IMDM from the outlet. After 5 min, 200 μL
260 IMDM containing the dyes (0.4 μL of 5 mM SYTO 9, 5 μL of 1.5 mM PI), 7.0×10^5 fluorescent
261 microbubbles (vMB lipid conjugate batch EU), and either 0, 0.1, or 1% of bovine serum albumin (BSA;
262 A9418-50G; Sigma-Aldrich) [45, 46] or casein (37582; Thermo Fisher Scientific) [47] was added to the
263 microchannel. μ -Slides were then flipped 180° for 5 min to allow the microbubbles to float up towards

264 the bottom of the microchannel for binding and then flipped back to their original position. Three binding
265 assays were performed for each condition. μ -Slides were systematically imaged with the 100 \times objective
266 (for specifics see subsection 2.4.1). The number of vMB attached to the bottom and top of the
267 microchannel was manually determined using Fiji software in 40 different field-of-view distributed over
268 the μ -Slide, divided in 20 fields-of-view located at the bottom and 20 fields-of view located at the top of
269 the microchannel. The binding efficiency was defined by the following formula:

$$270 \quad \text{Binding efficiency} = \frac{\text{Sum amount MBs bottom}}{\text{total amount MBs bottom and top}} \times 100\%$$

271 2.4.3 Microbubble binding under increasing shear stress

272 To exclude differences in results due to biofilm heterogeneity and possible variable biofilm erosion
273 under flow conditions, vMB (lipid conjugate batch EU) and DiI-containig cMB were simultaneously
274 added at a ratio of 1:1 to biofilms grown under flow at 5 dyn/cm². A solution of 200 μ L IMDM
275 containing 0.4 μ L of 5 mM SYTO 9 and 1.2×10^7 microbubbles was injected into the in-line Luer injection
276 port with a 1 mL Luer Solo syringe (Omnifix-F, B Braun, Melsungen, Germany) and 19G needle
277 (Sterican, B Braun) while the flow was turned off and the Ibidi μ -Slide was oriented upside down (Fig.
278 2D). To introduce microbubbles and SYTO 9 into the microchannel, a shear stress of 1.3 dyn/cm² (3.74
279 mL/min) was applied for 17 s. The vMB and cMB were then incubated with the biofilm for 5 min without
280 flow. Flow was started and increased every 60 s, with an initial shear stress increase of 0.5 dyn/cm² (1.43
281 mL/min), from 1.5 (4.33 mL/min) to 2 dyn/cm² (5.76 mL/min), and then each subsequent step was
282 increased by 1 dyn/cm² (\sim 2.87 mL/min) until 12 dyn/cm² (34.53 mL/min, Reynolds number: 74.2) was
283 achieved. The number of microbubbles remaining attached to the biofilm while applying increasing flows
284 was monitored with confocal time-lapse microscopy (0.77 frames per second (fps)) using a 60 \times water-
285 immersion objective (Plan Apo 60XA WI, Nikon Instruments) of which each field-of-view consisted of
286 512×512 pixels ($210 \times 210 \mu\text{m}^2$). The binding percentage was defined by the following formula:

$$287 \quad \text{Binding percentage} = \frac{\text{MBs bound after 60 s shear stress}}{\text{total amount MBs before flow}} \times 100\%$$

288 2.5 Sonobactericide with vancomycin-decorated microbubbles

289 2.5.1 Sonobactericide therapy

290 To biofilms grown under flow at 5 dyn/cm², a solution of 200 μL containing 0.4 μL of 5 mM SYTO 9,
291 5 μL of 1.5 mM PI and 1.2×10⁷ vMB (lipid conjugate batch EU) in IMDM was added into the in-line
292 Luer injection port as described above. After this, a continuous laminar flow of 5 dyn/cm² was applied to
293 the biofilm. For sonobactericide therapy, the clinically used transthoracic echocardiography frequency of
294 2 MHz was chosen [48]. Biofilms were insonified with ultrasound after a minimum of 50 s of continuous
295 flow exposure. A single 5,000- or 10,000-cycle burst at 250 kPa peak negative pressure was given,
296 resulting in a treatment time of 2.5 or 5 ms. For the ultrasound only control, a single 10,000-cycle burst at
297 250 kPa peak negative pressure was given. The spatial peak intensity (I_{SP}) was calculated by using the
298 formula: $I_{SP} = P^2/2\rho c$ [49, 50] where P denotes the peak pressure, ρ denotes the density and c the speed of
299 sound, resulting in a I_{SP} of 2.06 W/cm². All experiments were monitored for bacterial and vMB responses
300 with time-lapse confocal microscopy (0.77 fps) using the 60×objective (for specifics see subsection
301 2.4.3).

302 The biofilm reduction was quantified based on the SYTO 9 signal using a custom-built image analysis
303 code in MATLAB (The MathWorks, Natick, MA, USA). The area without biofilm was determined in a
304 frame before and within 15 s after ultrasound insonification, both selected based on minimal signal
305 variability due to focus drift. Images were first converted to binary by thresholding at 300 (image
306 intensity ranging from 0-4095). Next, all connected components were identified through the *bwconncomp*
307 function in MATLAB. All connected components with an area larger than 200 pixels (33.5 μm²) were
308 classified as areas without biofilm and normalized to the size of the field-of-view (512×512 pixels; 210 ×
309 210 μm²). The biofilm reduction was defined as the change in normalized area without biofilm before and
310 after ultrasound insonification.

311 2.5.2 *Brandaris 128* ultra-high-speed recordings

312 To resolve the oscillation behavior of the vMB (lipid conjugate batch EU) while bound to the bacterial
313 biofilm under flow at 5 dyn/cm^2 upon ultrasound exposure, the Brandaris 128 ultra-high-speed camera
314 was used as previously described [41]. Briefly, the Brandaris 128 was coupled to the custom-built Nikon
315 A1R+ confocal microscope, which made it possible to visualize both the microbubble behavior on a
316 microsecond time-scale and sonobactericide treatment effect after ultrasound exposure with high
317 resolution confocal microscopy. Time-lapse confocal imaging using the 100 \times objective (for specifics see
318 subsection 2.4.1) started during continuous flow (5 dyn/cm^2), capturing first the initial state of the biofilm
319 and bound vMB. For the Brandaris 128 ultra-high-speed camera recording, the light path was
320 automatically switched from the confocal scan head to the Brandaris 128 and was defined as $t = 0 \text{ s}$.
321 During ultrasound exposure (2 MHz, 250 kPa, 5,000 cycles), the first ~ 14 microbubble oscillations were
322 recorded in 128 frames at a framerate of 14.9 million fps. The microbubble diameter as a function of time
323 was subtracted from the Brandaris 128 recording using custom-designed software [51]. After obtaining all
324 128 frames, the light path was automatically switched back to the original position to continue confocal
325 time-lapse imaging. The biofilm reduction was quantified as described above with the exception that 544
326 pixels were taken for all connected components with an area larger than $33.5 \mu\text{m}^2$ to account for the
327 difference in magnification.

328 *2.6 Ultrasound molecular imaging*

329 A high frequency pre-clinical scanner (Vevo 3100, FUJIFILM VisualSonics, Toronto, Canada) was used
330 in combination with an ultra-high frequency linear array transducer (MX250, FUJIFILM VisualSonics)
331 operated at 18 MHz to visualize vMB bound to the biofilm. Biofilms were grown under flow at 5 dyn/cm^2
332 as described under 2.2.2. with the exception that the perfusion set was modified with the addition of an y-
333 style splitter (1.6 mm, 10828; Ibidi) placed 11.5 cm from the inlet of the μ -Slide. To the y-style splitter,
334 20 cm of additional biocompatible silicone tubing (1.6mm; 10828; Ibidi) was attached which was
335 clamped off during biofilm growth using a hose clip (10821; Ibidi). For the experiment, the flow by the
336 Ibidi pump system was stopped and the perfusion set clamped just after the additional y-style splitter.

337 Then, the tubing was cut just under the original y-style splitters on both sides of the perfusion set, the
338 additional tubing unclamped, and attached to a syringe pump (Pump 11 Elite, Harvard Apparatus,
339 Holliston, Massachusetts, USA) so that injected fluid and vMB passed the biofilm only once (Fig. 2E). A
340 solution of 200 μ L IMDM containing 1.2×10^7 vMB (lipid conjugate batch EU) and 1% BSA was added
341 into the in-line Luer injection port as described under 2.4.3. After 5 min of incubation, a shear stress of
342 1.5 dyn/cm^2 was applied for 60 s to remove unbound vMB from the biofilm. The transducer was operated
343 in a 7° angle at 10% transmit power, medium beamwidth and 40 dB dynamic range and manipulated
344 using a 3D acquisition motor (FUJIFILM VisualSonics) with a step size of 0.04 mm. Burst mode was
345 used 1, 5 and 10 times to locally destroy vMB. B-mode and non-linear contrast mode were used to
346 acquire images. Vevo LAB software was used to determine the mean contrast power and for rendering
347 volume projections of 6.52 mm non-linear contrast scans.

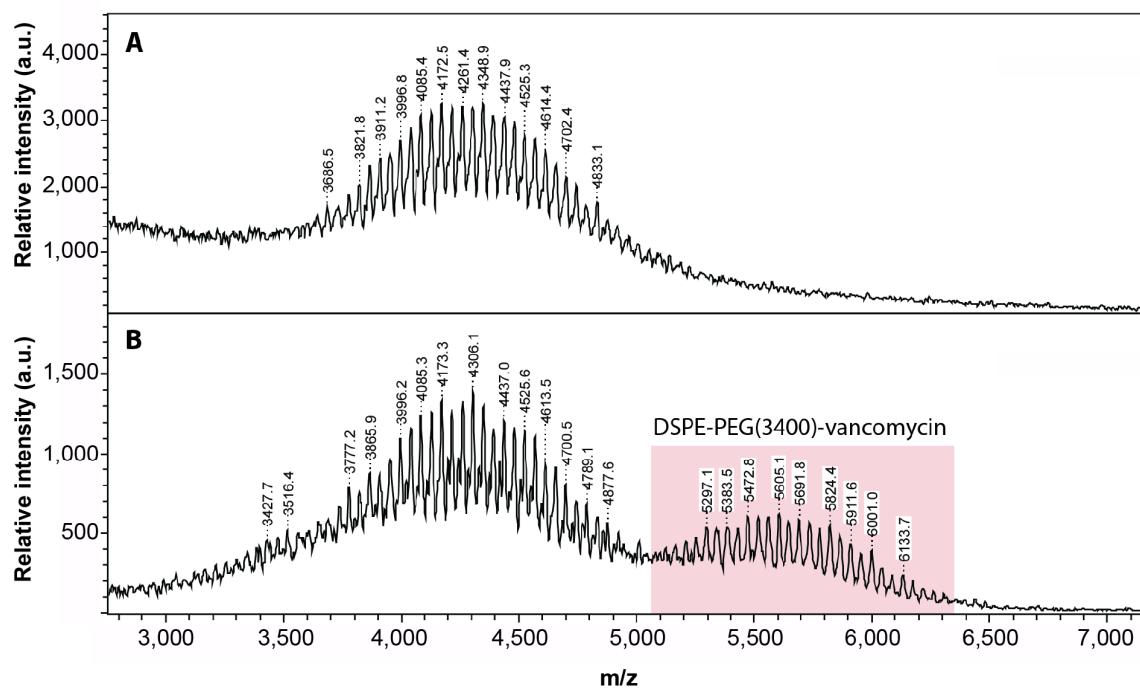
348 2.7 Statistical analysis

349 All data were statistically analyzed using IBM SPSS Statistics 27 (IBM Corporation, Armonk, New
350 York, USA), and a p -value of < 0.05 was used as the significance level. Data distribution was assessed
351 using the Shapiro-Wilk test. The data on the microbubble size distribution, competitive microbubble
352 binding assay, stability and microbubble binding under increasing shear stress was not normally
353 distributed and was compared by performing a Mann-Whitney U test. To further analyze the competitive
354 microbubble binding assay data, the Spearman's rank-order correlation was evaluated in MATLAB. The
355 sonobactericide therapy data was not normally distributed and the robust test of equality of means showed
356 to be significant, so a Welch's t-test was performed instead. Normally distributed data of the non-specific
357 vMB binding assay was compared using an unpaired t-test or one-way ANOVA with post-hoc Tukey
358 HSD test for multiple groups.

359 3. Results

360 3.1 Conjugation of vancomycin to phospholipid and incorporation in the microbubble shell

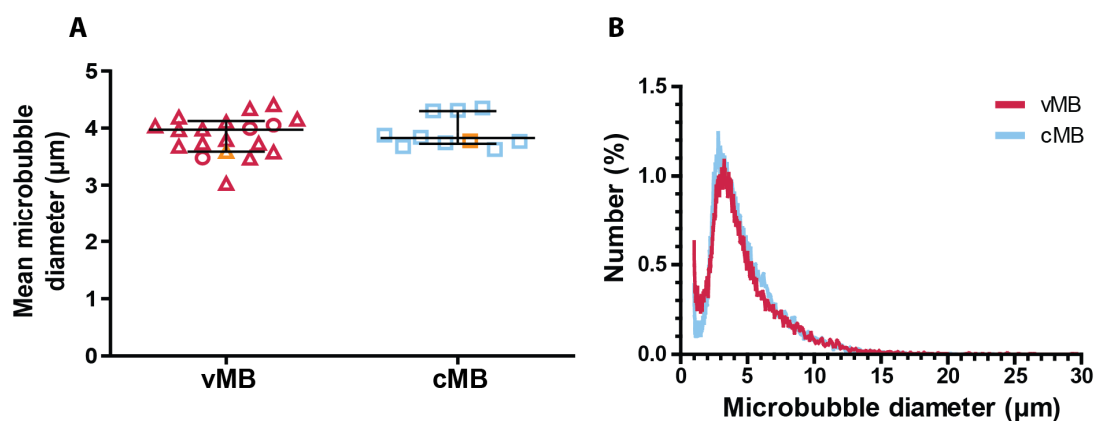
361 The freeze-dried product obtained after dialysis was analyzed by mass spectrometry in order to assess
362 the formation of the expected DSPE-PEG(3400)-vancomycin conjugate. Electrospray experiments were
363 performed on the freeze-dried product containing both the lipid and the expected lipid conjugate. The
364 multiplicity of PEG units in the lipid and the presence of the chlorine isotopes in vancomycin led to
365 intricate spectra where the average molecular weight (MW) determination of the conjugate was not
366 possible. According to MALDI-TOF experiments, the starting lipid was found to have a MW of ~4,260
367 (Fig. 3A). The presence of the starting lipid and a second compound with an average MW of 5,691,
368 matching with the expected conjugate of ~5,700, was confirmed for the freeze-dried product (Fig. 3B).
369 Successful conjugation between the DSPE-PEG(3400)-NHS and vancomycin was further confirmed by
370 TLC (Fig. S1).



371
372 **Fig. 3.** Matrix-assisted laser desorption/ionization - time-of-flight mass spectra of (A) DSPE-PEG(3400)
373 and (B) the freeze-dried product after dialysis with the red shaded region confirming the vancomycin
374 coupled to the polyethylene-glycol (PEG) lipid.

375

376 The number weighted mean diameter of the vMB produced with the lipid conjugate batch USA or
377 lipid batch conjugate EU did not show a significant difference between batches ($p = 0.737$). When
378 comparing the number weighted diameter of vMB (median: 3.97, interquartile range: 0.52) to cMB
379 diameter (median: 3.83, interquartile range: 0.58) (Fig. 4A), no significant difference was found ($p =$
380 0.604). The number weighted diameter of vMB does not indicate changes in microbubble size over the
381 three-day period in which the experiments were performed. Fig. 4B shows similar polydisperse
382 microbubble size distributions for vMB and cMB.

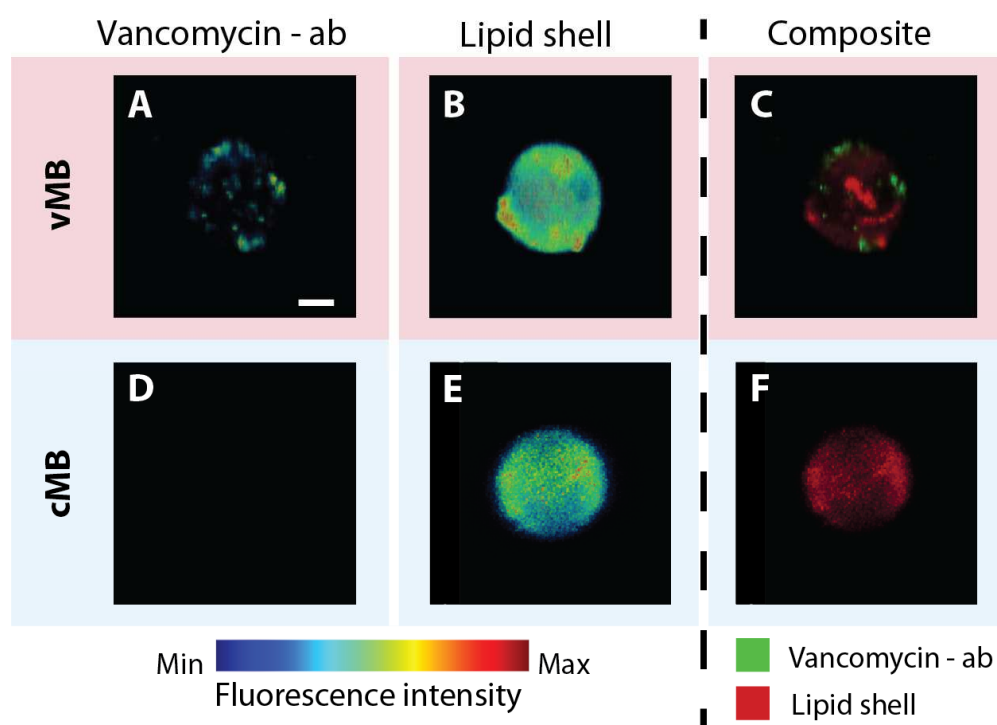


383

384 **Fig. 4.** Microbubble number-weighted mean diameter and size distribution. (A) The mean diameter of
385 vancomycin-decorated microbubbles (vMB, red, $n=19$ batches) and control microbubbles (cMB, blue,
386 $n=10$ batches) used in all experiments. The vMB were produced with either lipid conjugate batch USA
387 (red circles) or lipid conjugate batch EU (red triangles). The median and interquartile range are overlaid.
388 Orange-colored symbols indicate the MB batches corresponding to those represented in B. (B)
389 Representative size distribution of vMB and cMB batches.

390 Incubation of vMB with a FITC-labeled anti-vancomycin antibody confirmed the presence of
391 vancomycin as a ligand on the phospholipid coating using high-axial resolution 4Pi confocal microscopy.
392 The patch-like FITC-signal within the three-dimensional reconstruction of the vMB, as seen in Fig. 5A,

393 indicates that vancomycin is heterogeneously distributed over the vMB coating. The corresponding 4Pi
 394 confocal microscopy recording is shown in Video 1. The absence of any FITC-signal in the cMB (Fig.
 395 5D) shows that there was no non-specific binding of the FITC-labeled anti-vancomycin antibody to the
 396 other phospholipid components. The corresponding 4Pi confocal microscopy recording is shown in Video
 397 2. The destroyed freeze-dried vMB samples contained 3.23 and 2.69 $\mu\text{g}/\text{mL}$ of vancomycin,
 398 corresponding to an average of 0.035 μg of vancomycin per mg of destroyed freeze-dried vMB. The lipid
 399 conjugate samples contained 87.46 and 60.43 $\mu\text{g}/\text{mL}$ vancomycin, corresponding to an average of 41.41
 400 μg vancomycin per mg of lipid conjugate. The average vancomycin loading efficiency was calculated to
 401 be 0.71%. The average number of vancomycin molecules per μm^2 of microbubble shell was calculated to
 402 be 5358 (5285 and 5431 molecules).

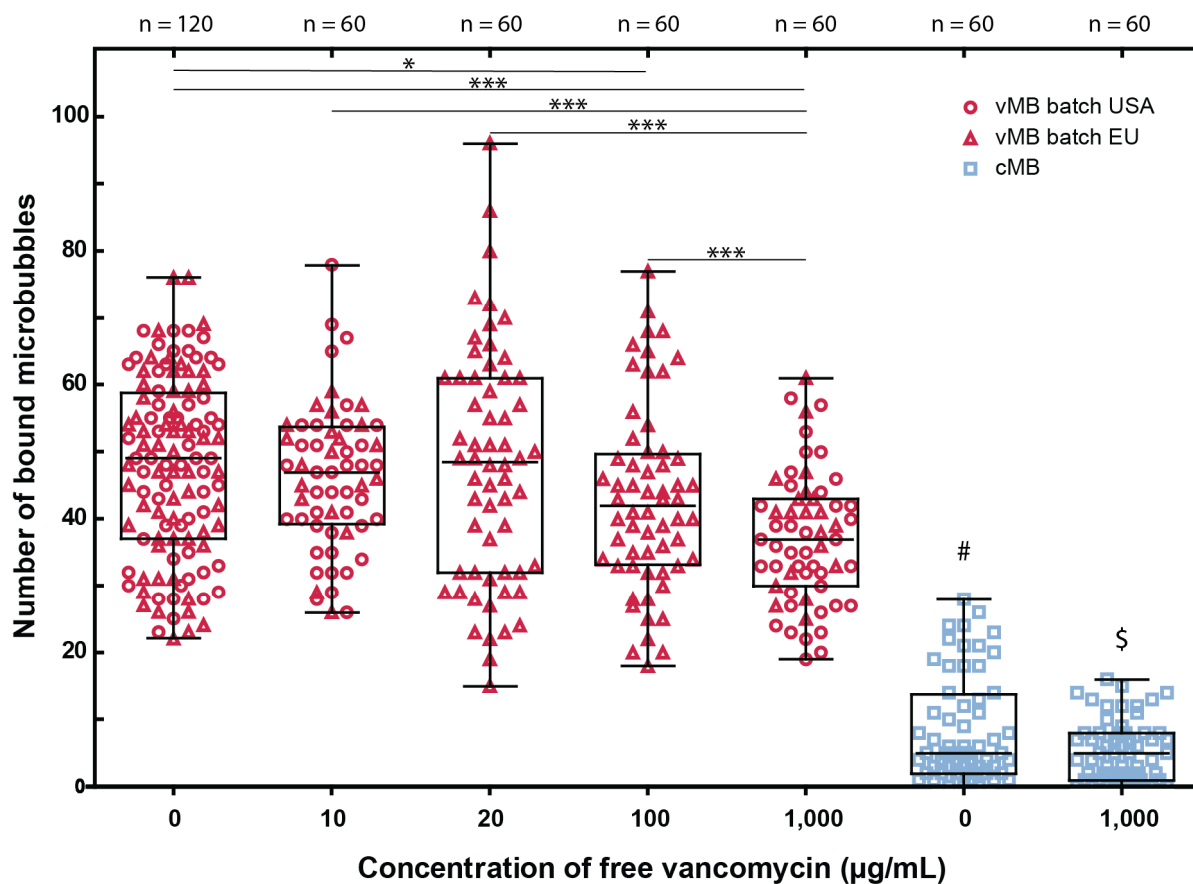


403
 404 **Fig. 5.** Representative 3D reconstructions of high-axial resolution 4Pi confocal microscopy y-stacks of
 405 (A-C) a vancomycin-decorated microbubble (vMB, diameter = 4.2 μm) and (D-F) a control microbubble
 406 (cMB, diameter = 4.3 μm). (A, D) Fluorescence intensity images of the FITC-labeled anti-vancomycin

407 antibody (vancomycin-ab) and (B, E) the phospholipid shells with the lipid dye DiD for vMB and DiI for
408 cMB. (C, F) The composite image of the fluorescence emitted by the FITC-labeled anti-vancomycin
409 antibody (green) and lipid dye (red). Scale bar is 1 μm and applies to all images.

410 *3.2 Binding of targeted microbubbles to bacteria in biofilms*

411 The ability of vMB and cMB to bind to statically grown biofilms was assessed with a competitive
412 microbubble binding assay (Fig. 6). Significantly more vMB were found at the bacterial biofilms
413 compared to cMB, regardless of the concentration of free vancomycin present. For vMB, increasing the
414 concentration of free vancomycin up to 20 $\mu\text{g}/\text{mL}$ prior to the incubation with vMB did not result in a
415 significant decrease in the amount of bound vMB. Only the preincubation of biofilms with a free
416 vancomycin concentration greatly exceeding the maximal clinical dose of 20 $\mu\text{g}/\text{mL}$, namely 100 and
417 1,000 $\mu\text{g}/\text{mL}$, reduced the number of bound vMB (respectively, $p = 0.02$ and $p < 0.001$). No significant
418 difference ($p = 0.74$) was found between the binding of vMB produced with either the USA or EU lipid
419 conjugate batch. There was no significant difference ($p = 0.065$) between the number of cMB after
420 preincubating without or with 1,000 $\mu\text{g}/\text{mL}$ of vancomycin. Furthermore, using the same data as in Fig. 6
421 the number of vMB and cMB was found to be unaffected by the location within the μ -Slides (Fig. S2). At
422 most a moderate negative correlation (i.e. number of microbubbles moderately decreases as the distance
423 from the inlet increases) was observed for two conditions, both with vMB, with a free vancomycin
424 concentration of 10 $\mu\text{g}/\text{mL}$ ($r = -0.53$, $p < 0.001$) and 1,000 $\mu\text{g}/\text{mL}$ ($r = -0.54$, $p < 0.001$). All other
425 conditions had coefficient values less than 0.4 (r values ranging from -0.33 to 0.13), which indicate little
426 to no relationship between the two variables. The stability of the vMB did not decrease during the three-
427 day period the microbubbles were used for experiments (Fig. S3). On day 3 there was even a slight but
428 significant increase in the number of bound vMB ($p < 0.05$).

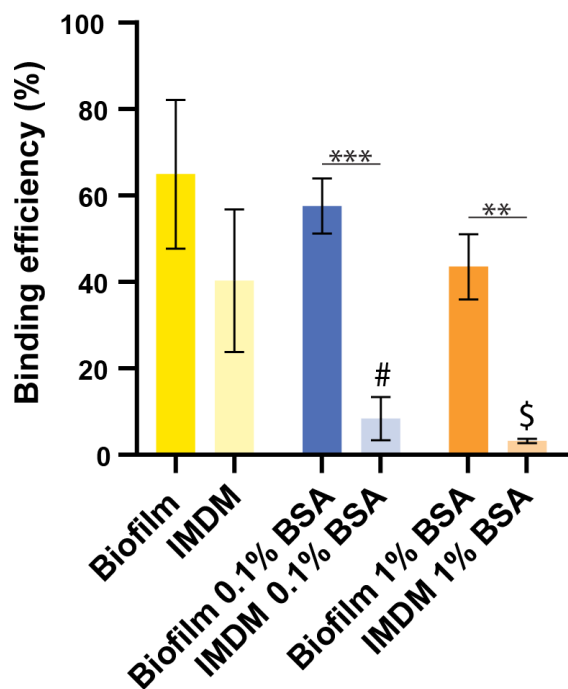


429

430 **Fig. 6.** The number of bound vancomycin-decorated (vMB, red symbols) and control (cMB, blue squares)
 431 for varying concentrations of free vancomycin with statically grown biofilms. The vMB were produced
 432 with either lipid conjugate batch USA (red circles) or batch EU (red triangles). Each symbol represents
 433 the number of microbubbles counted in one field-of-view. The overlaid boxplots show the median,
 434 interquartile range, and the minimum to maximum values. Statistical significance for vMB is indicated
 435 with * ($p < 0.05$) or *** ($p < 0.001$) when comparing different free vancomycin concentrations, # ($p <$
 436 0.001) when comparing cMB without free vancomycin to all vMB conditions, and \$ ($p < 0.001$) when
 437 comparing cMB with 1,000 µg/mL free vancomycin to all vMB conditions.

438 cMB showed negligible non-specific binding to the µ-Slides without biofilm. Fig. 7 shows that the
 439 percentage of vMB bound to the µ-Slide without biofilm was approximately two-thirds of the percentage
 440 of vMB bound to biofilms. When 0.1% BSA was added, the percentage of vMB bound to the µ-Slide

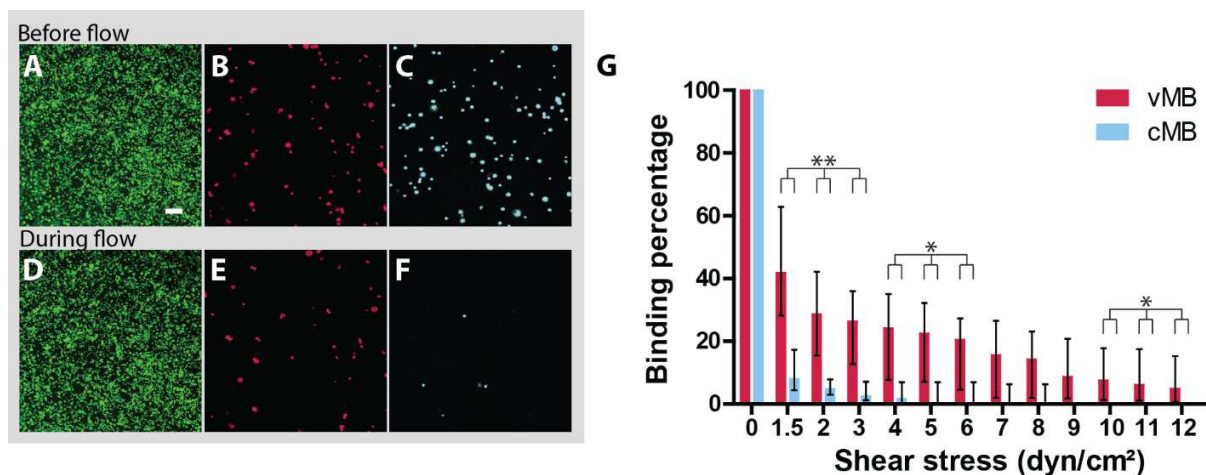
441 without biofilm significantly ($p < 0.05$) dropped while no significant changes ($p = 0.51$) were observed
 442 for the vMB bound to biofilms. When the BSA concentration was increased to 1%, the same trend was
 443 visible; a significant decrease of the percentage of vMB bound to the μ -Slide without biofilm ($p < 0.05$)
 444 and no significant differences ($p = 0.13$) for the percentage of vMB bound to the biofilm. Similar results
 445 were obtained when BSA was substituted for casein (Fig. S4).



446
 447 **Fig. 7.** Non-specific binding of vancomycin-decorated microbubbles. Ibidi μ -Slides with and without
 448 statically grown biofilms in IMDM were incubated with either 0 %, 0.1 % or 1% bovine serum albumin
 449 (BSA) to bind to non-specific binding sites. Each bar represents the mean binding efficiency percentage
 450 with standard deviation overlaid of $n=3$. Statistical significance is indicated with ** ($p < 0.01$), *** ($p <$
 451 0.001), # ($p < 0.05$) between IMDM 0.1% BSA and all other conditions except for IMDM 1% BSA, and \$
 452 ($p < 0.05$) between IMDM 1% BSA and all other conditions except for IMDM 0.1% BSA.

453 To determine the number of microbubbles that remained bound under flow, the vMB and cMB were
 454 distinguished by the different lipid dyes incorporated into their coating as shown in Fig. 8B, E and C, F,
 455 respectively. The average number of vMB present before flow was 51 ± 37 and for cMB 61 ± 44 (mean \pm

456 SD; n = 8) per field-of-view, and the ratio of vMB/cMB was 0.87 ± 0.16 . Time-lapse imaging while flow
 457 shear stress increased from 1.5 to 12 dyn/cm² was performed to distinguish bound from unbound
 458 microbubbles and revealed that vMB had a significantly higher binding percentage in comparison to cMB
 459 at all shear stress values, except from 7 to 9 dyn/cm² (Fig. 8G). The biofilm remained attached to the
 460 microchannel throughout the duration of flow binding experiments (Fig. 8A,D).

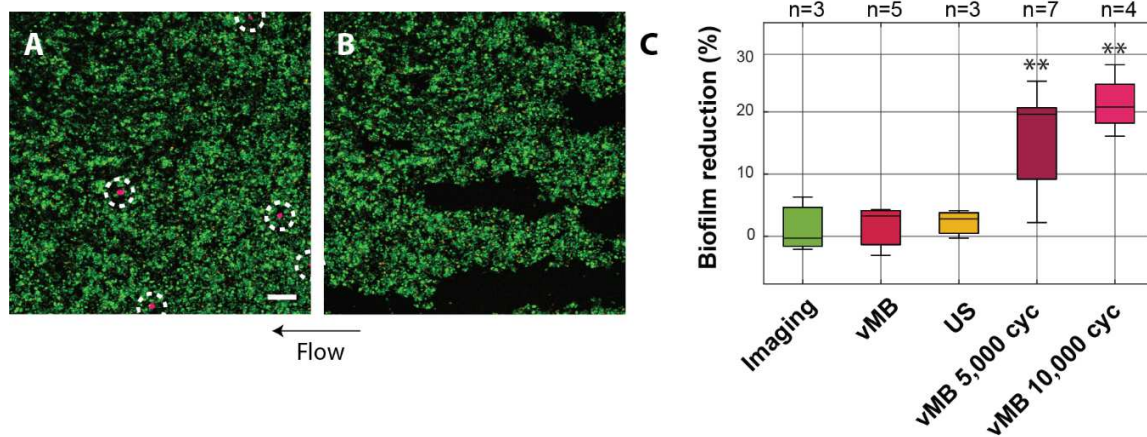


461 **Fig. 8.** Percentage of microbubbles that remained bound upon increasing shear stress with flow grown
 462 biofilms. Confocal microscopy images of (A-C) the initial state before flow and (D-F) after 60 s of 1.5
 463 dyn/cm² shear stress flow. Both sets of images are the same biofilm with (A, D) bacteria stained with
 464 SYTO 9 (green), (B, E) vancomycin-decorated microbubbles (vMB) stained with DiD (red), and (C, F)
 465 control microbubbles (cMB) stained with DiI (blue). Scale bar is 20 μm and applies to all confocal
 466 images. (G) Bars represent median percentage with interquartile range of microbubbles in the field-of-
 467 view remaining bound to the bacterial biofilm during increasing shear stress (n = 8). Statistical
 468 significance between bound vMB percentage and bound cMB percentage is indicated with * ($p < 0.05$) or
 469 ** ($p < 0.01$).

470 3.3 Sonobactericide with vancomycin-decorated microbubbles

471 Biofilms grown under flow had a field-of-view coverage of $89.7 \pm 10.7\%$ (mean \pm SD) (n=22 fields-
 472 of-view in 11 different μ-Slides). A typical example of a biofilm treated with sonobactericide using vMB

473 is shown in Fig. 9, where five vMB (diameter ranging from 2.0 to 4.5 μm) remained attached to the
 474 biofilm under flow (5 dyn/cm^2) before ultrasound treatment (Fig. 9A). Upon ultrasound insonification
 475 using 5,000 cycles, all vMB displaced from the field-of-view resulting in a 24.0% reduction in biofilm
 476 area localized along the microbubble displacement trajectories (Fig. 9B). The corresponding confocal
 477 microscopy recording is shown in Video 3. Overall, biofilms ($n = 7$) treated with vMB and a single
 478 ultrasound burst of 5,000 cycles resulted in a median reduction of 19.6% (interquartile range 11.5%; Fig.
 479 9C). When vMB were exposed to 10,000 cycles, a more consistent biofilm reduction amount was
 480 observed, with the highest being 27.6% and a median of 20.8% (interquartile range 6.3%; $n = 4$; Fig. 9C),
 481 albeit not significantly different from 5,000 cycles. No noticeable increase in PI positive cells was
 482 observed following all treatments. Both ultrasound settings in combination with vMB resulted in
 483 significantly higher biofilm area reduction than any of the control treatments (imaging under flow only,
 484 vMB only, and ultrasound only). Similar low percentages (<6.3%) of biofilm area reduction were
 485 obtained for all control treatments partly due to focus drift during the confocal microscopy recordings and
 486 biofilm erosion.



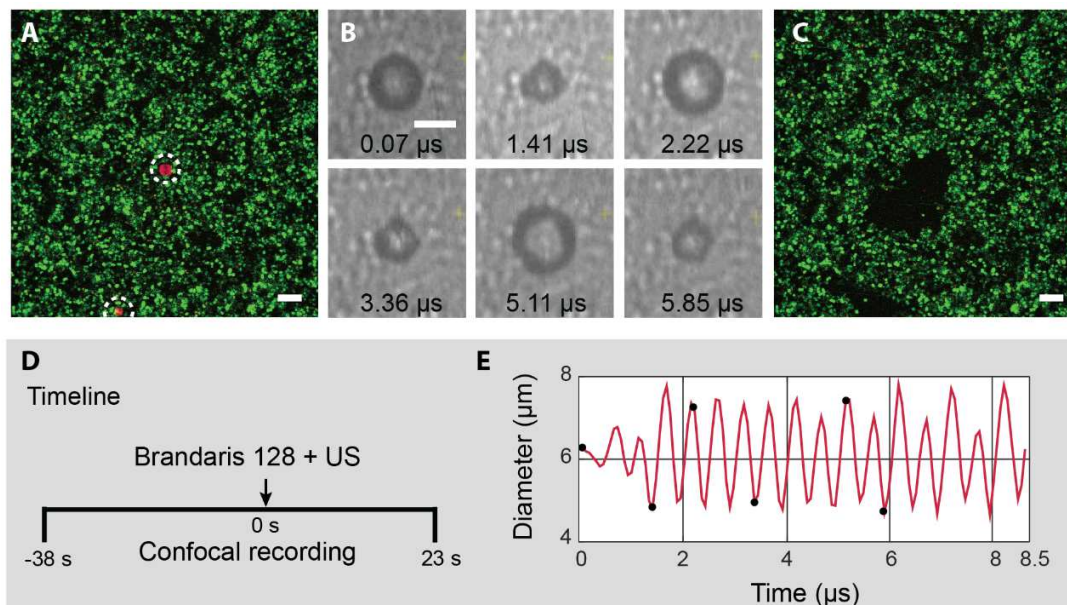
487

488 **Fig. 9.** Biofilms treated under flow at 5 dyn/cm^2 with vancomycin-decorated microbubbles (vMB) and
 489 ultrasound. Confocal microscopy images of (A) before and (B) after sonobactericide treatment (2 MHz,
 490 250 kPa, 5,000 cycles. Live bacteria were stained with SYTO 9 (green), dead bacteria with propidium
 491 iodide (orange), and vMB with DiD (red; indicated by white dashed circles). Scale bar is 20 μm and

492 applies to all confocal images. (C) Percentage of biofilm reduction upon treatment. Boxplots show the
493 median, interquartile range, and the minimum to maximum values. The ultrasound (US) setting of 2 MHz,
494 250 kPa, 10,000 cycles was used for US alone. Statistical significances between vMB in combination
495 with US and the control treatment groups are indicated with ** ($p < 0.01$); cyc = cycles.

496

497 To visualize the effect of the sonobactericide treatment on a microsecond time scale, Brandaris 128
498 ultra-high-speed camera recording was combined with time-lapse confocal microscopy. Fig. 10A shows
499 an example of a selected confocal microscopy frame of a biofilm with two vMB (diameter 6.3 μm and 4.3
500 μm) attached under flow before ultrasound insonification. During continuous flow, the vMB were
501 simultaneously insonified (5,000 cycles) and the largest vMB in the middle of the field-of-view recorded
502 at an ultra-high-speed for the first 14 cycles, where selected frames of this recording are shown in Fig.
503 10B. Throughout the Brandaris 128 recording (Fig. 10E), the vMB remained bound to the bacterial
504 biofilm and the microbubble oscillation amplitude was determined in each frame, resulting in a diameter
505 range from 4.7 μm to 7.8 μm during ultrasound exposure. The corresponding Brandaris 128 recording is
506 shown in Video 4. After ultrasound insonification, the effect of the oscillating vMB on the biofilm was
507 clearly visible (Fig. 10C), where approximately 606.1 μm^2 was removed, corresponding to a 3.7% total
508 reduction in the field-of-view. This reduction is within the range observed for this insonification as shown
509 in Fig. 9C, even though the magnification was higher.



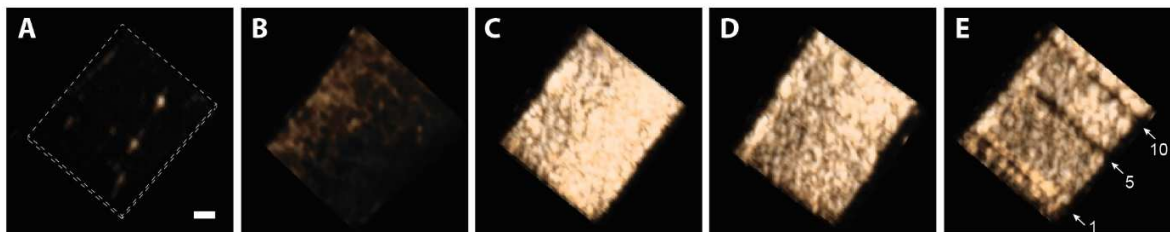
510

511 **Fig. 10.** Theranostic potential of vancomycin-decorated microbubble (vMB) upon ultrasound under flow
 512 (5 dyn/cm^2). (A) Initial state confocal microscopy image of vMB (red, DiD stained; indicated by white
 513 dashed circles) bound to bacteria (green, SYTO 9 stained) $\sim 1 \text{ s}$ before ultrasound exposure. Dead bacteria
 514 were stained with propidium iodide (orange). Scale bar is $10 \mu\text{m}$ and also applies to C. (B) Selected
 515 frames of Brandaris 128 ultra-high-speed camera recording showing the vMB in the center of A
 516 oscillating in response to a single burst of ultrasound (US; 2 MHz , 250 kPa , $5,000$ cycles). Scale bar is 5
 517 μm . (C) Corresponding confocal image $\sim 3 \text{ s}$ after ultrasound exposure showing biofilm disruption. (D)
 518 Imaging timeline during recordings. (E) Microbubble diameter as a function of time visualizing the
 519 oscillation behavior of the microbubble during ultrasound insonification. The black dots correspond to the
 520 selected images in B.

521 **3.4 Ultrasound molecular imaging**

522 B-mode images of μ -Slides without biofilm showed minimal ultrasonic signal compared to μ -Slides
 523 containing biofilms (Fig. S5). Non-linear contrast mode imaging showed only minimal signal for μ -Slides
 524 without biofilm (Fig. 11A). When a biofilm grown under flow was imaged in non-linear contrast mode,

525 thicker parts of the biofilm could be detected in the microchannel before the introduction of vMB (Fig.
526 11B). After incubation with vMB (Fig. 11C), the contrast-to-tissue ratio increased dramatically by 20.2
527 dB. The ultrasound molecular signal, with an 18.1 dB contrast-to-tissue ratio, only slightly decreased after
528 washing away unbound vMB (Fig. 11D). To confirm that the non-linear signal was generated by the
529 vMB, bursts were applied on three different places resulting in three individual lines across the 3D
530 rendered image (Fig. 11E) where the vMB were destroyed.



531

532 **Fig. 11.** Ultrasound molecular imaging of biofilm. 3D rendered non-linear contrast image of the
533 microchannel of a μ -Slide (A) without biofilm (microchannel delineated by the white dashed rectangle),
534 (B) with biofilm before addition of vancomycin-decorated microbubbles (vMB), (C) with biofilm after
535 incubation with vMB, (D) with biofilm after incubation and washing away unbound vMB, and (E) after
536 applying 1, 5 or 10 flash bursts (white arrows followed by 1, 5 and 10). Scale bar is 1 mm and applies to
537 all images.

538 4. Discussion

539 In this study, a novel targeted microbubble was successfully developed based on the NHS ester
540 chemical reaction that resulted in the coupling of the antibiotic vancomycin to the microbubble coating.
541 Furthermore, using bacteria-associated biofilms, ultrasound, and flow, the theranostic proof-of-principle
542 was demonstrated for the first time using a vMB and ultra-high-speed recording of the microbubble
543 oscillation behavior. Targeting microbubbles directly to biofilms has the potential to further enhance
544 therapy and provide a diagnostic component at the same time, both of which are desperately needed.

545 *4.1 Successful conjugation of vancomycin to phospholipid and incorporation in the microbubble shell*

546 The coupling of vancomycin to the microbubble phospholipid component DSPE-PEG(3400) was done
547 via the NHS ester functional group of the lipid and primary amine of the vancomycin, a method also used
548 by others for coupling vancomycin to a fluorescent dye [36]. MALDI-TOF mass spectrometry confirmed
549 successful conjugation, where the starting material only shows a peak at around ~4,260 Da and all
550 conjugated samples had a second peak at ~5,700 Da indicating the conjugate (Fig. 3). However, due to
551 the chloride isotopes of vancomycin and multiplicity of the lipid's PEG-tail, it was not possible to
552 determine the exact ratio between starting materials and final conjugate. The 4Pi microscopy data shows
553 that the vancomycin was heterogeneously distributed over the microbubble coating after production (Fig.
554 5). This heterogeneous ligand distribution might play a role in binding given that not every part of the
555 microbubble coating can bind to bacteria. Although heterogeneous ligand distributions have previously
556 been reported for DSPC-based microbubbles [52, 53], a more homogeneous distribution could increase
557 the probability of the vMB to bind to the bacteria. Lipid handling prior to microbubble production [54] or
558 different heating-cooling protocols after microbubble production [53] have been shown to alter ligand
559 distribution to become homogeneous in DSPC-based microbubbles, but these require organic solvents or
560 high temperatures which may compromise vancomycin functionality. One of the possibilities to improve
561 the binding profile of the vMB is to expand the purification process of the lipid conjugate after dialysis.

562 The antimicrobial property of vancomycin coupled to a microbubble coating should still be present
563 since the binding site used to inhibit cell wall synthesis remains intact after conjugation. The overall
564 therapeutic effect of the conjugated vancomycin alone is then only limited by the amount that is coupled
565 and how many bacteria can bind to each microbubble. **By determining the vancomycin concentration on**
566 **the vMB, the amount of vancomycin in a clinical dose of 1×10^9 vMB [55] was calculated to be 0.78 μg .**
567 This is extremely low when considering the clinical target serum concentration of vancomycin is 15-20
568 $\mu\text{g/ml}$ [43, 44]. **On the other hand, the calculated average number of 5358 vancomycin molecules per μm^2**
569 **of microbubble shell is in the similar range as the previously reported ~2500 antibody molecules for P-**

570 **selectin targeted lipid coated microbubbles [56]**. Although microbubble coating coverage is crucial when
571 considering it may increase chances of microbubble binding *in vivo*, the therapeutic enhancement effects
572 that vMB can provide lies more on the ultrasound-mediated microbubble behavior. This includes the
573 potential to decrease the current dosage of vancomycin necessary for patients, which could lower the
574 incidence of antibiotic-induced nephrotoxicity.

575 4.2 Successful binding of targeted microbubbles to bacteria in biofilms

576 Almost all sonobactericide studies use static biofilm cultivation [26]. For some research questions and
577 target diseases, static biofilms are adequate. However, to also include flow-related biofilm-mediated
578 diseases, the addition of multiple flow shear stresses to the biofilm model was pivotal. This addition, in
579 combination with the human plasma coating, resulted in differently grown biofilms which often had a
580 more three-dimensional structure to it than statically grown biofilms. Our vMB successfully bound to
581 bacteria and remained bound through increasing shear stresses of up to 12 dyn/cm² (Fig. 8). Although the
582 maximal shear stress used in this *in vitro* model is on the lower spectrum in healthy human arteries (10-70
583 dyn/cm²), it is above the shear stress found in healthy veins (1-6 dyn/cm²) [57]. Binding of targeted
584 microbubbles under high shear stress conditions can be challenging. To bypass this problem, one could
585 make use of primary acoustic radiation forces. *Dayton et al.* [58] and *Rychak et al.* [47, 59] showed that
586 this phenomenon increases microbubble binding in flow conditions by displacing microbubbles towards
587 the desired binding area *in vitro* and *in vivo*, while also significantly reducing the flow speed of these
588 microbubbles. Theoretically, this approach can increase the number of targeted microbubbles binding to
589 biofilms. Another consideration is that the circulatory system experiences pulsatile flow with each
590 heartbeat. The lull between each cyclical increase and decrease in flow and the forwards and backwards
591 motion of fluid, both due to pulsatile flow, could provide enough time for vMB to bind compared to a
592 continuous flow state. It therefore is of interest for future studies to investigate binding under flow using
593 ultrasound and pulsatile flow, potentially providing an even better binding profile of vMB.

594 A factor that could affect vMB binding success is that patients are started on antibiotic therapy the
595 moment infection is suspected, which means that the available binding sites could already be occupied
596 before vMB are administered. Therefore, competition was assessed using free vancomycin concentrations
597 ranging from 0 to 1,000 $\mu\text{g/ml}$ (Fig. 6), and no significant differences were observed between 0 and 20
598 $\mu\text{g/ml}$, which is the clinical dose. This lends support that vMB can still be used as a theranostic whether
599 or not the patient is already on high-concentration vancomycin therapy. Another factor which can also
600 affect vMB efficiency is plasma protein binding. For free vancomycin, this has been reported as
601 approximately 26% [60], which could also be the case for vMB. It is also possible that if vancomycin is
602 administered to the patient before vMB are infused, it could minimize the off-target binding to plasma
603 proteins and other potential non-desired attachment. Nonetheless, experiments need to be performed in
604 order to make this determination.

605 Variability was seen in the number of bound vMB (Fig. 6), which partly could be explained by the
606 heterogenous nature of biofilms, such as differences in the amount and accessibility of the D-Ala-D-Ala
607 moiety of the bacteria in the biofilm. This relation between binding of targeted microbubbles and the
608 density of the biomarker is clearly demonstrated by *Takalkar et al.* [56] in their *in vitro* study using anti
609 P-selectin antibody microbubbles and P-selectin as biomarker. Likely, this variability can also partly be
610 explained by the fluctuation in the number of microbubbles entering the microchannel of the Ibidi μ -
611 Slide. Regardless, the number of bound vMB for each condition was all significantly higher than the cMB
612 groups. cMB did exhibit some non-specific binding to the biofilm (Fig. 6), however this was minor and
613 known to also occur with non-targeted microbubbles for mammalian cells [61-63]. Under flow conditions
614 the cMB adherence to biofilms, for example at 1.5 dyn/cm^2 (Fig. 8G), could in fact be due to the natural
615 rough, irregular surface of biofilms preventing microbubbles from moving away and requiring a certain
616 level of flow to overcome this. cMB binding results were significantly different than vMB, both in
617 number of microbubbles bound statically and in their ability to withstand flow, except for 7 to 9 dyn/cm^2
618 which could also be explained by microbubbles getting stuck in the biofilm's irregular surface (e.g.,
619 protuberances) without binding. Higher flow shear stresses remove the residual unbound control

620 microbubbles from the irregular surface while vMB remained bound. To minimize the effect
621 heterogenous biofilms could have on the binding percentage, both vMB and cMB were tested together in
622 the flow experiments at a 1:1 ratio. However, the ratio in the fields-of-view was found to be 0.87:1, and
623 therefore the percentage in the microbubble binding under increasing shear stress represents a smaller
624 number of vMB compared to cMB. It is possible that vMB could have bound to bacteria potentially
625 growing within the tubing set or inlet, and/or planktonic bacteria in the media before reaching the field-
626 of-view within the μ -Slides resulting in the lower amount of vMB in comparison to cMB.

627 The non-specific binding of vMB found in μ -Slides only containing IMDM, i.e. without biofilm, (Fig.
628 7) was likely due to electrostatic non-specific binding to the microchannel of the μ -Slide. When 0.1% or
629 1% BSA was added to the vMB solution, this non-specific binding was significantly decreased while
630 maintaining the specific binding to the bacterial biofilm. No similar non-specific binding is expected *in*
631 *vivo*, since human serum albumin is abundantly present in the bloodstream, i.e. up to 5.5% [64].

632 4.3 Theranostic proof-of-principle of vancomycin-decorated microbubbles

633 This study provides diagnostic and therapeutic proof-of-principle by showing vMB response upon
634 ultrasound insonification. The ability of bound vMB to biofilms to generate an echogenic signal in non-
635 linear contrast mode (Fig. 11) shows vMB could be used to detect early biofilm development via
636 ultrasound molecular imaging, for which up till now no single suitable detection method is available.
637 Using the Brandaris 128 ultra-high-speed camera, a vMB under flow was shown to exhibit oscillations
638 upon insonification while staying bound to the biofilm (Fig. 10). Concerning therapeutic potential, vMB
639 bound to bacteria were able to significantly disrupt biofilms when exposed to ultrasound (Fig. 8). This
640 conforms to other reports from sonobactericide papers where non-targeted microbubbles combined with
641 ultrasound can have a therapeutic effect on *in vitro* and *in vivo* biofilms [65]. However, this study
642 revealed some different biofilm reduction effects which might be contributed to targeted microbubbles
643 and flow. Specifically, the streak pattern and large amount of reduction caused by individual
644 microbubbles and one burst of ultrasound versus the craters and holes that others report by concentrated

645 non-targeted microbubbles and different insonification schemes. Biofilm reduction was most likely
646 caused by the microbubble oscillatory mechanical effects (Fig. 10), such as microstreaming in
647 combination with flow. Regardless of the mechanism, damaged biofilms become more sensitive to
648 antibiotics [66], which could translate to shorter duration and lower dosage of antibiotics needed to
649 achieve biofilm eradication.

650 Direct bacterial killing could also occur and in a manner of two avenues. Firstly, the vancomycin on
651 vMB bound to bacteria still has the ability to kill via the same mechanisms as free vancomycin. Secondly,
652 ultrasound-induced microbubble behavior could enhance membrane permeabilization ultimately leading
653 to cell death, as observed in mammalian cells [67]. The PI fluorescence stain is commonly used as a
654 marker of cell death, as used in this study to assess the initial state of bacteria within biofilms, but also as
655 a permeabilization marker since it is cell impermeable to intact membranes. However, direct PI uptake
656 after sonobactericide treatment was not observed in this study. This could be due to bacterial cells
657 requiring more time to die following membrane damage and dispersed cells not being trackable outside of
658 the field-of-view, since other studies report higher PI positive cell numbers but only seen by optical
659 imaging minutes to days after insonification [65]. The therapeutic impact of one bound vMB is probably
660 multifaceted, with direct and indirect consequences on both the bacteria and biofilm structure.

661 While this new approach shows promise to improve biofilm infection patient outcomes, it needs to be
662 certain that vMB do not contribute to bacterial dispersal and or the release of biofilm fragments into the
663 circulation. Bacteria that are dispersed or dislodged from biofilms due to vMB should be characterized to
664 understand and be able to address the potential risks to be viable as a therapeutic [66, 68]. For vMB as a
665 diagnostic, less risk is envisioned since the ultrasound settings used would remain within a few cycles and
666 on the lower acoustic pressure spectrum not intended to induce major bioeffects. **It is expected that the**
667 **vMB itself will not contribute to adverse effects. The main compound, DSPC, is also the main component**
668 **of SonoVue microbubbles which are already safely used in the clinic for several decades [69]. PEG-40**
669 **stearate is widely used as an emulsifier in microbubble formulations [70-72]. The gas used to produce the**
670 **vMB, C₄F₁₀, is a component of Sonazoid, another clinically approved microbubble [73]. Although in this**

671 study DSPE-PEG(3400) was used to couple vancomycin, the comparable DSPE-PEG(2000) is a
672 component of the BR55 microbubble, which has shown safety in clinical trials [29]. Vancomycin as an
673 antibiotic is used in the clinic with minimal side-effects [74].

674 **5. Conclusion**

675 In this study, to the best of our knowledge for the first time, vMB were produced and characterized
676 which showed successful incorporation of the antibiotic vancomycin to the microbubble's lipid shell.
677 Confocal microscopy revealed that vMB were able to bind to *S. aureus* biofilms and remained attached
678 under increasing physiological flow conditions. Significant biofilm reduction was seen upon ultrasound-
679 activation of vMB. vMB oscillation under flow was visualized on a microsecond time-scale using the
680 Brandaris 128 ultra-high-speed camera. Bound vMB to the biofilm evidently enhanced the ultrasound
681 signal during ultrasound molecular imaging. The ability of vMB to bind to biofilms combined with the
682 mechanical effects induced upon ultrasound insonification have promising potential to both enhance
683 treatment through sonobactericide and provide early diagnosis by ultrasound molecular imaging of
684 biofilm-mediated diseases.

685 **Acknowledgements**

686 This project has received funding from the European Research Council (ERC) under the European
687 Union's Horizon 2020 research and innovation program [grant agreement 805308]. Gaëtan Mislin
688 acknowledges the Interdisciplinary Thematic Institute (ITI) InnoVec (Innovative Vectorization of
689 Biomolecules, IdEx, ANR-10-IDEX-0002) and SFRI (ANR-20-SFRI-0012). The authors would like to
690 thank Robert Beurskens, Frits Mastik and Reza Pakdaman Zangabad from the Department of Biomedical
691 Engineering, Michiel Manten from the Department of Experimental Medical Instrumentation, Andi R.
692 Sultan from the Department of Medical Microbiology and Infectious Diseases and Ruud Huisman from
693 the Department of Hospital Pharmacy, all from the Erasmus University Medical Center Rotterdam, for

694 their skillful technical assistance. The authors thank the Optical Imaging Centre of Erasmus MC for the
695 use of their facilities and Gert van Cappellen and Alex Nigg for their help. The authors also thank the
696 members of the Therapeutic Ultrasound Contrast Agent group (Biomedical Engineering Dept.) and the *S.*
697 *aureus* working group (Medical Microbiology and Infectious Diseases Dept.) from Erasmus University
698 Medical Center Rotterdam for their useful discussions.

699 **Competing Interests**

700 The authors have declared that no competing interest exists.

701 References

- 702 1. Health, N.I.o., *Research on Microbial Biofilms. Report No. PA-03-047*. 2002.
- 703 2. Mah, T.F. and G.A. O'Toole, *Mechanisms of biofilm resistance to antimicrobial agents*. Trends
704 Microbiol, 2001. **9**(1): p. 34-9 DOI: 10.1016/s0966-842x(00)01913-2.
- 705 3. Waters, E.M., et al., *Convergence of Staphylococcus aureus Persister and Biofilm Research: Can*
706 *Biofilms Be Defined as Communities of Adherent Persister Cells?* PLoS Pathog, 2016. **12**(12): p.
707 e1006012 DOI: 10.1371/journal.ppat.1006012.
- 708 4. Stewart, P.S. and J.W. Costerton, *Antibiotic resistance of bacteria in biofilms*. Lancet, 2001.
709 **358**(9276): p. 135-8.
- 710 5. Ito, A., et al., *Increased antibiotic resistance of Escherichia coli in mature biofilms*. Appl Environ
711 Microbiol, 2009. **75**(12): p. 4093-100 DOI: 10.1128/AEM.02949-08.
- 712 6. Lewis, K., *Persister cells and the riddle of biofilm survival*. Biochemistry (Mosc), 2005. **70**(2): p.
713 267-74.
- 714 7. Cassini, A., et al., *Attributable deaths and disability-adjusted life-years caused by infections with*
715 *antibiotic-resistant bacteria in the EU and the European Economic Area in 2015: a population-*
716 *level modelling analysis*. Lancet Infect Dis, 2019. **19**(1): p. 56-66 DOI: 10.1016/S1473-
717 3099(18)30605-4.
- 718 8. Lee, S.W., et al., *How microbes read the map: Effects of implant topography on bacterial*
719 *adhesion and biofilm formation*. Biomaterials, 2021. **268**: p. 120595 DOI:
720 10.1016/j.biomaterials.2020.120595.
- 721 9. Chirouze, C., et al., *Prognostic factors in 61 cases of Staphylococcus aureus prosthetic valve*
722 *infective endocarditis from the International Collaboration on Endocarditis merged database*.
723 Clin Infect Dis, 2004. **38**(9): p. 1323-7 DOI: 10.1086/383035.
- 724 10. Murdoch, D.R., et al., *Clinical presentation, etiology, and outcome of infective endocarditis in the*
725 *21st century: the International Collaboration on Endocarditis-Pro prospective Cohort Study*. Arch
726 Intern Med, 2009. **169**(5): p. 463-73 DOI: 10.1001/archinternmed.2008.603.
- 727 11. Mirabel, M., et al., *Long-term outcomes and cardiac surgery in critically ill patients with infective*
728 *endocarditis*. Eur Heart J, 2014. **35**(18): p. 1195-204 DOI: 10.1093/eurheartj/ehf303.
- 729 12. Bannay, A., et al., *The impact of valve surgery on short- and long-term mortality in left-sided*
730 *infective endocarditis: do differences in methodological approaches explain previous conflicting*
731 *results?* Eur Heart J, 2011. **32**(16): p. 2003-15 DOI: 10.1093/eurheartj/ehp008.
- 732 13. Bin Abdulhak, A.A., et al., *Global and regional burden of infective endocarditis, 1990-2010: a*
733 *systematic review of the literature*. Glob Heart, 2014. **9**(1): p. 131-43 DOI:
734 10.1016/j.gheart.2014.01.002.
- 735 14. Tahon, J., et al., *Long-term follow-up of patients with infective endocarditis in a tertiary referral*
736 *center*. International Journal of Cardiology, 2021. **331**: p. 176-182.
- 737 15. DeSimone, D.C. and M.R. Sohail, *Management of bacteremia in patients living with*
738 *cardiovascular implantable electronic devices*. Heart Rhythm, 2016. **13**(11): p. 2247-2252 DOI:
739 10.1016/j.hrthm.2016.08.029.
- 740 16. Kreitmann, L., et al., *Clinical Characteristics and Outcome of Patients with Infective Endocarditis*
741 *Diagnosed in a Department of Internal Medicine*. J Clin Med, 2020. **9**(3) DOI:
742 10.3390/jcm9030864.
- 743 17. Kooiman, K., et al., *Acoustic behavior of microbubbles and implications for drug delivery*. Adv
744 Drug Deliv Rev, 2014. **72**: p. 28-48 DOI: 10.1016/j.addr.2014.03.003.

- 745 18. Daeichin, V., et al., *Microbubble Composition and Preparation for High-Frequency Contrast-*
746 *Enhanced Ultrasound Imaging: In Vitro and In Vivo Evaluation.* IEEE Trans Ultrason Ferroelectr
747 Freq Control, 2017. **64**(3): p. 555-567 DOI: 10.1109/TUFFC.2016.2640342.
- 748 19. Kooiman, K., et al., *Ultrasound-Responsive Cavitation Nuclei for Therapy and Drug Delivery.*
749 *Ultrasound Med Biol*, 2020. **46**(6): p. 1296-1325 DOI: 10.1016/j.ultrasmedbio.2020.01.002.
- 750 20. Sennoga, C.A., et al., *Microbubble-mediated ultrasound drug-delivery and therapeutic*
751 *monitoring.* Expert Opin Drug Deliv, 2017. **14**(9): p. 1031-1043 DOI:
752 10.1080/17425247.2017.1266328.
- 753 21. Schinkel, A.F.L., et al., *Contrast-Enhanced Ultrasound to Assess Carotid Intraplaque*
754 *Neovascularization.* *Ultrasound Med Biol*, 2020. **46**(3): p. 466-478 DOI:
755 10.1016/j.ultrasmedbio.2019.10.020.
- 756 22. Dimcevski, G., et al., *A human clinical trial using ultrasound and microbubbles to enhance*
757 *gemcitabine treatment of inoperable pancreatic cancer.* J Control Release, 2016. **243**: p. 172-181
758 DOI: 10.1016/j.jconrel.2016.10.007.
- 759 23. Kotopoulis, S., et al., *Treatment of human pancreatic cancer using combined ultrasound,*
760 *microbubbles, and gemcitabine: a clinical case study.* Med Phys, 2013. **40**(7): p. 072902 DOI:
761 10.1118/1.4808149.
- 762 24. Lipsman, N., et al., *Blood-brain barrier opening in Alzheimer's disease using MR-guided focused*
763 *ultrasound.* Nat Commun, 2018. **9**(1): p. 2336 DOI: 10.1038/s41467-018-04529-6.
- 764 25. Mainprize, T., et al., *Blood-Brain Barrier Opening in Primary Brain Tumors with Non-invasive MR-*
765 *Guided Focused Ultrasound: A Clinical Safety and Feasibility Study.* Sci Rep, 2019. **9**(1): p. 321
766 DOI: 10.1038/s41598-018-36340-0.
- 767 26. Lattwein, K.R., et al., *Sonobactericide: An Emerging Treatment Strategy for Bacterial Infections.*
768 *Ultrasound Med Biol*, 2020. **46**(2): p. 193-215 DOI: 10.1016/j.ultrasmedbio.2019.09.011.
- 769 27. Kosareva, A., et al., *Seeing the Invisible-Ultrasound Molecular Imaging.* *Ultrasound Med Biol*,
770 2020. **46**(3): p. 479-497 DOI: 10.1016/j.ultrasmedbio.2019.11.007.
- 771 28. Moccetti, F., et al., *Ultrasound Molecular Imaging of Atherosclerosis Using Small-Peptide*
772 *Targeting Ligands Against Endothelial Markers of Inflammation and Oxidative Stress.* *Ultrasound*
773 *Med Biol*, 2018. **44**(6): p. 1155-1163 DOI: 10.1016/j.ultrasmedbio.2018.01.001.
- 774 29. Willmann, J.K., et al., *Ultrasound Molecular Imaging With BR55 in Patients With Breast and*
775 *Ovarian Lesions: First-in-Human Results.* J Clin Oncol, 2017. **35**(19): p. 2133-2140 DOI:
776 10.1200/JCO.2016.70.8594.
- 777 30. Smeenge, M., et al., *First-in-Human Ultrasound Molecular Imaging With a VEGFR2-Specific*
778 *Ultrasound Molecular Contrast Agent (BR55) in Prostate Cancer: A Safety and Feasibility Pilot*
779 *Study.* Invest Radiol, 2017. **52**(7): p. 419-427 DOI: 10.1097/RLI.0000000000000362.
- 780 31. van Rooij, T., et al., *Targeted ultrasound contrast agents for ultrasound molecular imaging and*
781 *therapy.* Int J Hyperthermia, 2015. **31**(2): p. 90-106 DOI: 10.3109/02656736.2014.997809.
- 782 32. Anastasiadis, P., et al., *Detection and quantification of bacterial biofilms combining high-*
783 *frequency acoustic microscopy and targeted lipid microparticles.* J Nanobiotechnology, 2014. **12**:
784 p. 24 DOI: 10.1186/1477-3155-12-24.
- 785 33. Gilboa-Garber, N. and D. Sudakevitz, *The hemagglutinating activities of Pseudomonas*
786 *aeruginosa lectins PA-IL and PA-III exhibit opposite temperature profiles due to different*
787 *receptor types.* FEMS Immunol Med Microbiol, 1999. **25**(4): p. 365-9 DOI: 10.1111/j.1574-
788 695X.1999.tb01361.x.
- 789 34. Broker, B.M., S. Holtfreter, and I. Bekeredjian-Ding, *Immune control of Staphylococcus aureus -*
790 *regulation and counter-regulation of the adaptive immune response.* Int J Med Microbiol, 2014.
791 **304**(2): p. 204-14 DOI: 10.1016/j.ijmm.2013.11.008.

- 792 35. Wang, F., et al., *Insights into Key Interactions between Vancomycin and Bacterial Cell Wall*
793 *Structures*. ACS Omega, 2018. **3**(1): p. 37-45 DOI: 10.1021/acsomega.7b01483.
- 794 36. van Oosten, M., et al., *Real-time in vivo imaging of invasive- and biomaterial-associated*
795 *bacterial infections using fluorescently labelled vancomycin*. Nat Commun, 2013. **4**: p. 2584 DOI:
796 10.1038/ncomms3584.
- 797 37. Unnikrishnan, S., et al., *Formation of Microbubbles for Targeted Ultrasound Contrast Imaging:*
798 *Practical Translation Considerations*. Langmuir, 2019. **35**(31): p. 10034-10041 DOI:
799 10.1021/acs.langmuir.8b03551.
- 800 38. McComas, C.C., B.M. Crowley, and D.L. Boger, *Partitioning the loss in vancomycin binding affinity*
801 *for D-Ala-D-Lac into lost H-bond and repulsive lone pair contributions*. Journal of the American
802 Chemical Society, 2003. **125**(31): p. 9314-9315.
- 803 39. Dauty, E., et al., *Intracellular delivery of nanometric DNA particles via the folate receptor*.
804 Bioconjug Chem, 2002. **13**(4): p. 831-9 DOI: 10.1021/bc0255182.
- 805 40. Klibanov, A.L., et al., *Detection of individual microbubbles of ultrasound contrast agents: imaging*
806 *of free-floating and targeted bubbles*. Invest Radiol, 2004. **39**(3): p. 187-95 DOI:
807 10.1097/01.rli.0000115926.96796.75.
- 808 41. Beekers, I., et al., *Combined Confocal Microscope and Brandaaris 128 Ultra-High-Speed Camera*.
809 Ultrasound Med Biol, 2019. **45**(9): p. 2575-2582 DOI: 10.1016/j.ultrasmedbio.2019.06.004.
- 810 42. Chen, X., et al., *Ultra-fast bright field and fluorescence imaging of the dynamics of micrometer-*
811 *sized objects*. Rev Sci Instrum, 2013. **84**(6): p. 063701 DOI: 10.1063/1.4809168.
- 812 43. Pritchard, L., et al., *Increasing vancomycin serum trough concentrations and incidence of*
813 *nephrotoxicity*. Am J Med, 2010. **123**(12): p. 1143-9 DOI: 10.1016/j.amjmed.2010.07.025.
- 814 44. Tongchai, S. and P. Koomanachai, *The safety and efficacy of high versus low vancomycin trough*
815 *levels in the treatment of patients with infections caused by methicillin-resistant Staphylococcus*
816 *aureus: a meta-analysis*. BMC Res Notes, 2016. **9**(1): p. 455 DOI: 10.1186/s13104-016-2252-7.
- 817 45. Langeveld, S.A.G., et al., *The Impact of Lipid Handling and Phase Distribution on the Acoustic*
818 *Behavior of Microbubbles*. Pharmaceutics, 2021. **13**(1) DOI: 10.3390/pharmaceutics13010119.
- 819 46. Kooiman, K., et al., *Focal areas of increased lipid concentration on the coating of microbubbles*
820 *during short tone-burst ultrasound insonification*. PLoS One, 2017. **12**(7): p. e0180747 DOI:
821 10.1371/journal.pone.0180747.
- 822 47. Rychak, J.J., A.L. Klibanov, and J.A. Hossack, *Acoustic radiation force enhances targeted delivery*
823 *of ultrasound contrast microbubbles: in vitro verification*. IEEE Trans Ultrason Ferroelectr Freq
824 Control, 2005. **52**(3): p. 421-33 DOI: 10.1109/tuffc.2005.1417264.
- 825 48. Kremkau, F.W., *General principles of echocardiography*. ASE's Compr. Echocardiogr. 2015.
- 826 49. Merritt, C.R., F.W. Kremkau, and J.C. Hobbins, *Diagnostic ultrasound: bioeffects and safety*.
827 Ultrasound Obstet Gynecol, 1992. **2**(5): p. 366-74 DOI: 10.1046/j.1469-0705.1992.02050366.x.
- 828 50. Kinsler, L.E., et al., *Fundamentals of acoustics*. 2000: John Wiley & Sons.
- 829 51. van der Meer, S.M., et al., *Microbubble spectroscopy of ultrasound contrast agents*. J Acoust Soc
830 Am, 2007. **121**(1): p. 648-56 DOI: 10.1121/1.2390673.
- 831 52. Kooiman, K., et al., *DSPC or DPPC as main shell component influences ligand distribution and*
832 *binding area of lipid-coated targeted microbubbles*. European Journal of Lipid Science and
833 Technology, 2014. **116**(9): p. 1217-1227 DOI: 10.1002/ejlt.201300434.
- 834 53. Borden, M.A., et al., *Lateral phase separation in lipid-coated microbubbles*. Langmuir, 2006.
835 **22**(9): p. 4291-7 DOI: 10.1021/la052841v.
- 836 54. Langeveld, S.A.G., et al., *Ligand Distribution and Lipid Phase Behavior in Phospholipid-Coated*
837 *Microbubbles and Monolayers*. Langmuir, 2020. **36**(12): p. 3221-3233 DOI:
838 10.1021/acs.langmuir.9b03912.
- 839 55. *Lumason Safety Label FDA*. Center for Drug Evaluation and Research, Silver Spring, MD, USA

- 841 2016.
- 842 56. Takalkar, A.M., et al., *Binding and detachment dynamics of microbubbles targeted to P-selectin*
 843 *under controlled shear flow*. J Control Release, 2004. **96**(3): p. 473-82 DOI:
 844 10.1016/j.jconrel.2004.03.002.
- 845 57. Malek, A.M., S.L. Alper, and S. Izumo, *Hemodynamic shear stress and its role in atherosclerosis*.
 846 JAMA, 1999. **282**(21): p. 2035-42 DOI: 10.1001/jama.282.21.2035.
- 847 58. Dayton, P., et al., *Acoustic radiation force in vivo: a mechanism to assist targeting of*
 848 *microbubbles*. Ultrasound Med Biol, 1999. **25**(8): p. 1195-201 DOI: 10.1016/s0301-
 849 5629(99)00062-9.
- 850 59. Rychak, J.J., et al., *Enhanced targeting of ultrasound contrast agents using acoustic radiation*
 851 *force*. Ultrasound Med Biol, 2007. **33**(7): p. 1132-9 DOI: 10.1016/j.ultrasmedbio.2007.01.005.
- 852 60. Stove, V., et al., *Measuring Unbound Versus Total Vancomycin Concentrations in Serum and*
 853 *Plasma: Methodological Issues and Relevance*. Therapeutic Drug Monitoring, 2015. **37**(2).
- 854 61. Bettinger, T., et al., *Ultrasound molecular imaging contrast agent binding to both E- and P-*
 855 *selectin in different species*. Invest Radiol, 2012. **47**(9): p. 516-23 DOI:
 856 10.1097/RLI.0b013e31825cc605.
- 857 62. Wang, S., et al., *Ultra-Low-Dose Ultrasound Molecular Imaging for the Detection of Angiogenesis*
 858 *in a Mouse Murine Tumor Model: How Little Can We See?* Invest Radiol, 2016. **51**(12): p. 758-766
 859 DOI: 10.1097/RLI.0000000000000310.
- 860 63. Daeichin, V., et al., *Quantification of Endothelial alphavbeta3 Expression with High-Frequency*
 861 *Ultrasound and Targeted Microbubbles: In Vitro and In Vivo Studies*. Ultrasound Med Biol, 2016.
 862 **42**(9): p. 2283-93 DOI: 10.1016/j.ultrasmedbio.2016.05.005.
- 863 64. Burtis, C.A. and D.E. Bruns, *Tietz fundamentals of clinical chemistry and molecular diagnostics-e-*
 864 *book*. 2014: Elsevier Health Sciences.
- 865 65. Lattwein, K.R., et al., *Sonobactericide: An Emerging Treatment Strategy for Bacterial Infections*.
 866 Ultrasound in Medicine & Biology, 2020. **46**(2): p. 193-215 DOI:
 867 <https://doi.org/10.1016/j.ultrasmedbio.2019.09.011>.
- 868 66. Wille, J. and T. Coenye, *Biofilm dispersion: The key to biofilm eradication or opening Pandora's*
 869 *box?* Biofilm, 2020. **2**: p. 100027 DOI: <https://doi.org/10.1016/j.biofilm.2020.100027>.
- 870 67. van Rooij, T., et al., *Viability of endothelial cells after ultrasound-mediated sonoporation:*
 871 *Influence of targeting, oscillation, and displacement of microbubbles*. Journal of controlled
 872 release : official journal of the Controlled Release Society, 2016. **238**: p. 197-211 DOI:
 873 10.1016/j.jconrel.2016.07.037.
- 874 68. Franca, A., et al., *Characterization of an in vitro fed-batch model to obtain cells released from S.*
 875 *epidermidis biofilms*. AMB Express, 2016. **6**(1): p. 23 DOI: 10.1186/s13568-016-0197-9.
- 876 69. Lv, K., et al., *Prospective assessment of diagnostic efficacy and safety of SonazoidTM and*
 877 *SonoVue[®] ultrasound contrast agents in patients with focal liver lesions*. Abdominal Radiology,
 878 2021: p. 1-13.
- 879 70. Owen, J., et al., *The Role of PEG-40-stearate in the Production, Morphology, and Stability of*
 880 *Microbubbles*. Langmuir, 2018. **35**(31): p. 10014-10024.
- 881 71. Xing, Z., et al., *Novel ultrasound contrast agent based on microbubbles generated from*
 882 *surfactant mixtures of Span 60 and polyoxyethylene 40 stearate*. Acta biomaterialia, 2010. **6**(9):
 883 p. 3542-3549.
- 884 72. Dixon, A.J., et al., *Enhanced intracellular delivery of a model drug using microbubbles produced*
 885 *by a microfluidic device*. Ultrasound in medicine & biology, 2013. **39**(7): p. 1267-1276.

- 886 73. Chou, Y.H., et al., *Safety of Perfluorobutane (Sonazoid) in Characterizing Focal Liver Lesions*. J
887 Med Ultrasound, 2019. **27**(2): p. 81-85 DOI: 10.4103/JMU.JMU_44_19.
- 888 74. Rubinstein, E. and Y. Keynan, *Vancomycin revisited - 60 years later*. Front Public Health, 2014. **2**:
889 p. 217 DOI: 10.3389/fpubh.2014.00217.

890

891

892

893

894

895

896

897

898

899

900 **Video captions**

901 **Video 1.** Representative 3D reconstruction of high-axial resolution 4Pi confocal microscopy y-stacks of a
902 vancomycin-decorated microbubble (corresponding to Fig. 5A-C, diameter = 4.2 μm). Top left shows the
903 FITC-labeled anti-vancomycin antibody and on the top right the lipid dye. The pseudo-colored composite
904 view on the bottom left shows the FITC-labeled anti-vancomycin antibody in green and the lipid dye in
905 red.

906 **Video 2.** Representative 3D reconstruction of high-axial resolution 4Pi confocal microscopy y-stacks of a
907 control microbubble (corresponding to Fig. 5D-F, diameter = 4.3 μm). Top left shows the FITC-labeled
908 anti-vancomycin antibody (no signal) and on the top right the lipid dye. The pseudo-colored composite
909 view on the bottom left shows the FITC-labeled anti-vancomycin antibody in green (no signal) and the
910 lipid dye in red.

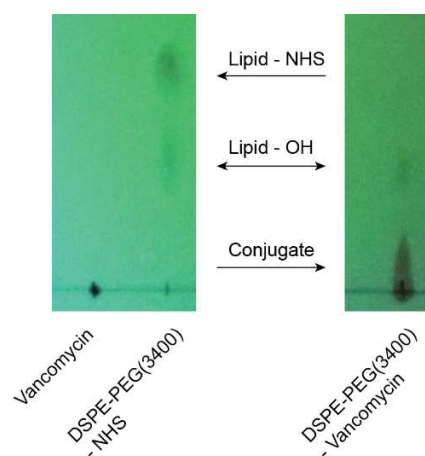
911 **Video 3.** Time-lapse confocal microscopy imaging showing biofilm reduction under flow shear stress of 5
912 dyn/cm^2 after ultrasound insonification of vancomycin-decorated microbubbles (corresponding to Fig.
913 9A,B). The pseudo-colored video shows live bacteria in green, dead bacteria in orange and vancomycin-
914 decorated microbubbles in red.

915 **Video 4.** Brandaris 128 ultra-high-speed recording (14.9 million frames per second) showing oscillations
916 of a single vancomycin-decorated microbubble bound to the biofilm under flow shear stress of 5 dyn/cm^2
917 (corresponding to Fig. 10B). Ultrasound insonification (2 MHz, 250 kPa peak negative pressure, 5,000
918 cycles) occurred at the 0.20 μs timestamp.

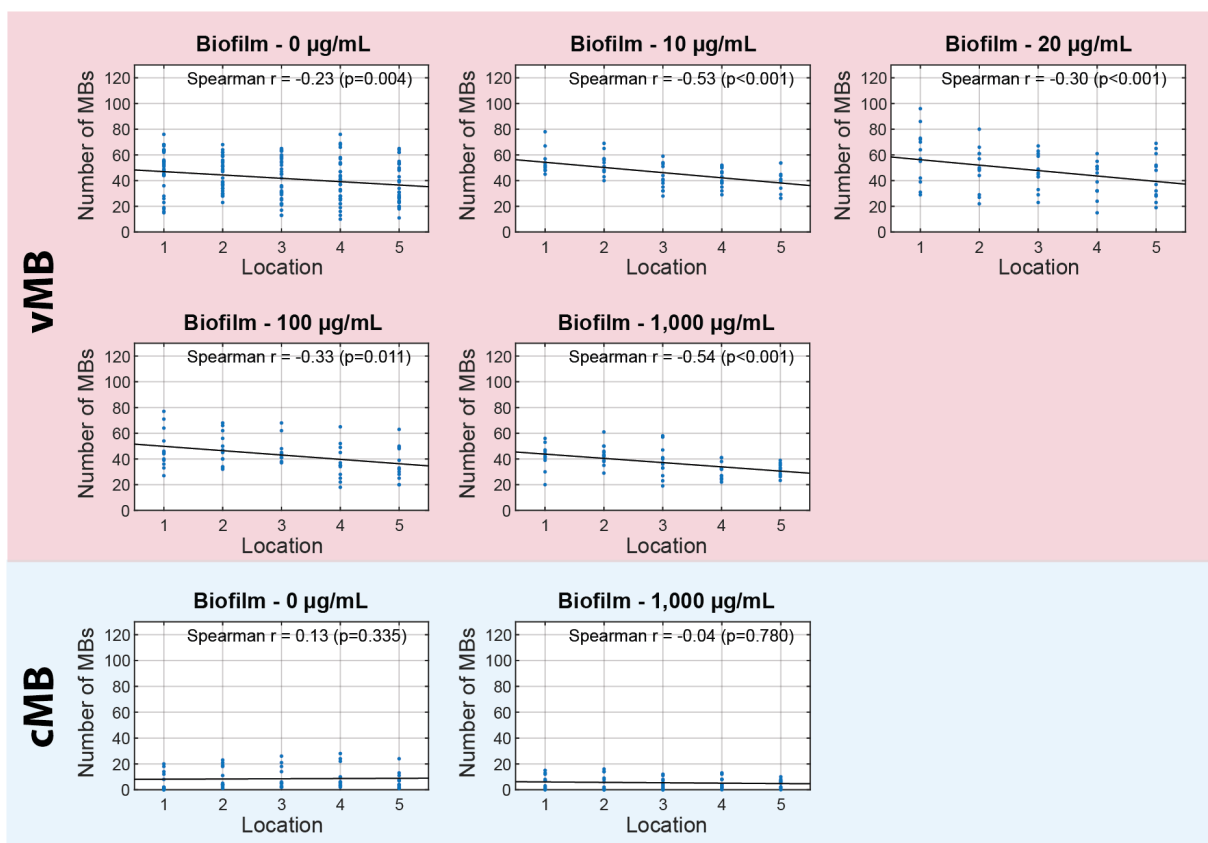
1 **Supplementary material for**

2 **Vancomycin-decorated microbubbles as a**
3 **theranostic agent for *Staphylococcus aureus***
4 **biofilms**

5
6 Joop J.P. Kouijzer, Kirby R. Lattwein, Inés Beekers, Simone A.G. Langeveld, Mariël Leon-
7 Grooters, Jean-Marc Strub, Estefania Oliva, Gaëtan L.A. Mislin, Nico de Jong, Antonius F.W.
8 van der Steen1, Alexander L. Klibanov, Willem J.B. van Wamel, Klazina Kooiman

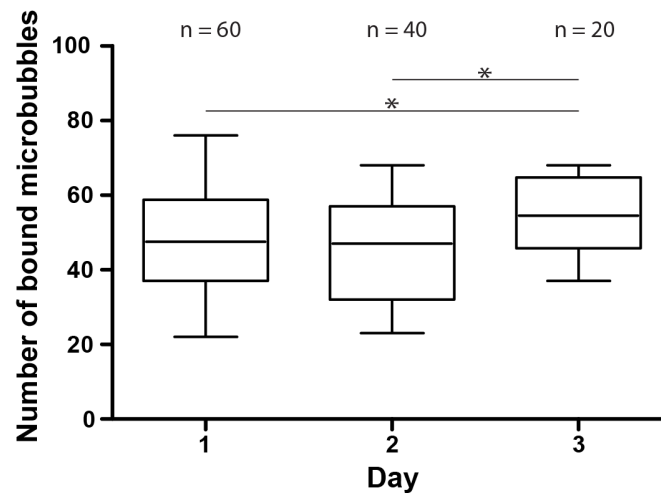


9
10 **Fig. S1.** Vancomycin coupling to the DSPE-PEG(3400)-NHS lipid. Thin-layer chromatography (TLC)
11 visualized the main components of the conjugation before the chemical reaction (left). Vancomycin did
12 not migrate, while DSPE-PEG(3400)-NHS did migrate and separated into two components: an unreacted
13 part (Lipid-NHS) and a hydrolyzed part (Lipid-OH). After the conjugation, TLC reveals the chemically
14 coupled end product after dialysis and freeze-drying (right). The hydrolyzed unreacted Lipid-OH remains
15 visible while the Lipid-NHS has reacted with the vancomycin and is not present anymore. Lipid-NHS is
16 DSPE-PEG(3400)-NHS; Lipid-OH is hydrolyzed DSPE-PEG(3400); conjugate is DSPE-PEG(3400)-
17 vancomycin.



18

19 **Fig. S2.** Scatter plots visualizing the relationship between the number of bound microbubbles (MBs) for
 20 vancomycin-decorated microbubbles (vMB) or control microbubbles (cMB) and their location within μ -
 21 Slides with statically grown biofilms and free vancomycin (0 – 1,000 $\mu\text{g/mL}$). The blue circles are the
 22 experimental data points, and the lines represent the best fit, with correlation assessed using the
 23 Spearman's correlation coefficient (r). Location 1 – 5 were equally spaced, with 1 representing the field-
 24 of view nearest to the inlet and 5 nearest to the outlet.



25

26 **Fig. S3.** The number of bound vancomycin-decorated microbubbles (vMB) in μ -Slides with statically
 27 grown biofilms over the three-day period the vMB were used for experiments. The boxplots show the
 28 median, interquartile range, and the minimum to maximum values. Statistical significance between the
 29 number of bound vMB on different days is indicated with * ($p < 0.05$).

30

31

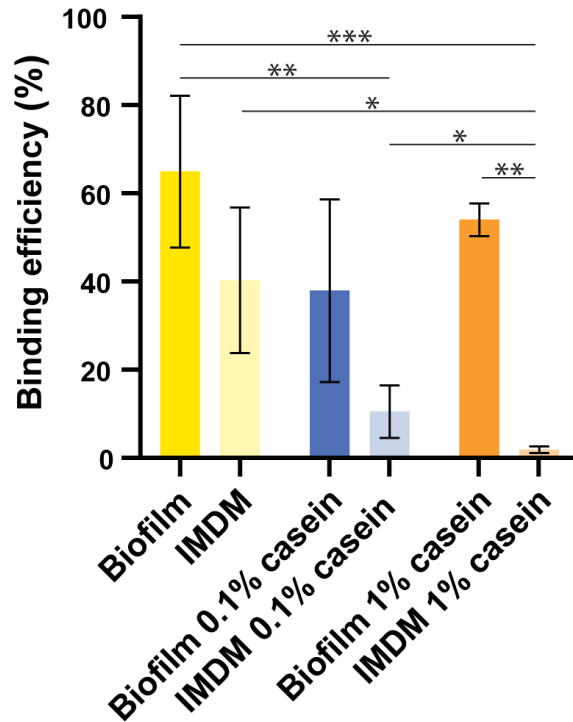
32

33

34

35

36



37

38 **Fig. S4.** Non-specific binding of vancomycin-decorated microbubbles. μ -Slides with and without
 39 statically grown biofilms in IMDM were incubated with either 0, 0.1 % or 1% casein to bind to non-
 40 specific binding sites. Each bar represents the mean binding efficiency percentage with standard deviation
 41 overlaid of n=3. Statistical significance is indicated with * ($p < 0.05$), ** ($p < 0.01$) or *** ($p < 0.001$).

42

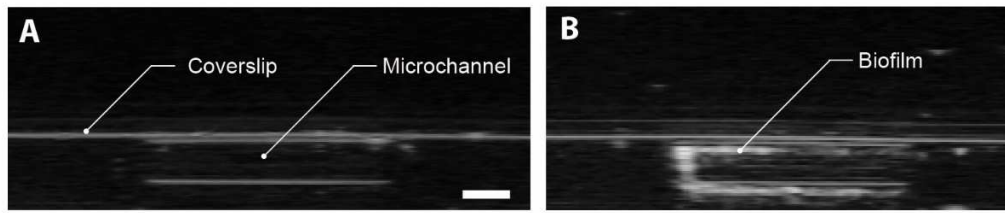
43

44

45

46

47



48

49 **Fig. S5.** B-mode imaging of a μ -Slide. Cross-section of a μ -Slide (A) without biofilm, and (B) with
50 biofilm grown under flow. Scale bar is 1 mm and applies to both images.